



IGC Newsletter

IN THIS ISSUE

Technical Articles

- Performance Testing of Primary Ramp and Primary Tilting Mechanism of Inclined Fuel Transfer Machine of Prototype Fast Breeder Reactor
- Science of Metal Nanoclusters

Young Officer's Forum

- Design of Elliptical Heat Exchanger for Future Fast Breeder Reactors

Young Researcher's Forum

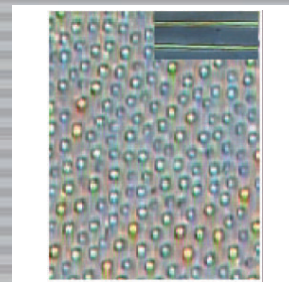
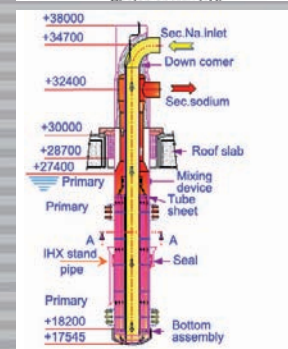
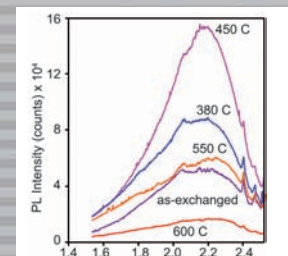
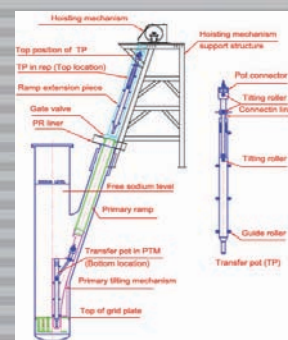
- Enhanced Transmission with Tunable Fano like Profile in Magnetic Soft Matter

Conference/Meeting Highlights

- Theme Meeting on Severe Accident Analysis and Experiments
- Theme Meeting on Robust Instrumentation and Control for Nuclear Facilities
- Theme Meeting on Technological Advancement in Production of Enriched Boron for the Control Rods of Fast Reactors

Visit of Dignitaries

Awards & Honours



From the Editor

Dear Reader

It is my pleasant privilege to forward a copy of the latest issue of IGC Newsletter (Volume 93, July 2012 issue).

In the Director's Desk, Shri S. C. Chetal, Director, IGCAR has highlighted the contributions made by Chemistry Group towards supporting the fast reactor programme and closing the fuel cycle. The significant inputs provided by the Group in the last five years like fuel-fission product interaction studies, development of failed fuel detection system, production of useful radioisotopes, development of chemical sensors, decontamination and sodium cleaning studies, boron chemistry, cover gas purification system, studies related to fuel cycle with special emphasis on metallic fuel fabrication, separation studies, waste immobilization and other important research activities towards unravelling the basics in chemistry.

Shri B.K. Sridhar and Shri S. Raghupathy have shared their experience on successful completion of the performance testing of primary ramp and primary tilting mechanism in air and sodium, and the effective in situ removal of sodium from primary ramp and primary tilting mechanism by water vapor and carbon dioxide process.

In the second technical article, Dr. P. Gangopadhyay has discussed the Science of Metal Nanoclusters by analyzing and interpreting the results of the photoluminescence, optical absorption spectroscopy and Rutherford backscattering experiments of silver ion-exchanged/implanted soda-glass samples and Raman scattering spectroscopy of cobalt implanted silica samples.

In the young officer's forum, Shri V. Sudharshan gave an account of optimising the configuration of intermediate heat exchanger for economy and designed an elliptical heat exchanger for future fast breeder reactors with design life of 60 years at 85% load factor.

Dr. Junaid Masud Laskar, in the young researcher's account, has presented the first experimental evidence for tunable fano resonance in magnetically polarizable soft matter system and explained the variation of different fano parameters with external magnetic field on the basis of change in interference due to varying waveguide dimension and their dimensional distributions.

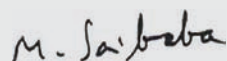
This Newsletter carries reports on the Theme Meetings on "Severe Accident Analysis and Experiments", "Robust Instrumentation and Control for Nuclear Facilities" and "Technological Advancement in Production of Enriched Boron for the Control Rods of Fast Reactors".

Honorable Justice Shri S. Tamilvanan from Madras High Court and Prof. V. Manimozhi visited the Centre during the last quarter.

We are happy to share with you the awards, honours and distinctions earned by our colleagues. We look forward to your feedback, continued guidance and support.

With my best wishes and personal regards,

Yours sincerely,



(M. Sai Baba)

Chairman, Editorial Committee, IGC Newsletter

&

Associate Director, Resources Management Group

Director's Desk



Chemistry Programme at IGCAR

The importance of chemistry as a key discipline in the development of fast reactor technology and the fuel cycle was recognised by our department in the very early stages of the fast reactor programme. The Radiochemistry Laboratory (RCL) was one of the first set of laboratories built at IGCAR. At that stage, the chemistry laboratory was intended to provide support for the development of the fast reactor programme through R&D activities related to fuel materials, liquid sodium and other alkali metals, and the fuel cycle for fast reactor. Over the years, the Chemistry Group (CG) has not only met this mandate, but also has provided key technological inputs to several other aspects of the fast reactor programme. The work on plutonium chemistry was initiated in the year 1983. The historical evolution of the chemistry programme at IGCAR and the contributions of CG in the first 25 years were covered in the article that appeared in the newsletter in April 2005. In the present article, I have focused more on the achievements of CG in the subsequent period, while providing some idea of the earlier work in order to present a comprehensive perspective.

CONTRIBUTIONS TO FBTR

The Chemistry Group provided key inputs to the decision on the composition of the carbide fuel for FBTR. The knowledge base on the thermochemical properties of the fuel and fission product systems, and the strengths in thermochemical modeling were instrumental in arriving at an understanding of the chemical state of the carbide fuel at high burn-up. This was particularly necessary for extension of the burn-up of FBTR fuel beyond 150 GWD/t. The equilibration experiments carried out to study the chemical interaction of $(U_{0.56}Pu_{0.44})O_{2-x}$ with liquid sodium were useful in obtaining safety clearance for the introduction of plutonium rich oxide fuel in FBTR.

Chemistry Group was also responsible for the characterization

of the sodium that was charged into FBTR and the chemical characterization of various structural materials. Over the years, the group has continued to provide characterization support for the sodium coolant in FBTR. Various impurities in sodium have been measured periodically, and gamma spectrometry measurements have been carried out on radioactive sodium from the primary sodium loop of FBTR.

The Chemistry Group was involved in the development of a failed fuel detection system for FBTR, based on the measurement of Kr^{87}/Kr^{85} and Kr^{88}/Kr^{85} ratios in the cover gas by gamma spectrometry. This development proved to be crucial in the localization of the failed fuel in FBTR, in the first incidence of carbide fuel pin failure. The measurement of the krypton isotope ratios combined with the reactor power history led to an estimate of the age of failed fuel and burn-up of the breached sub-assembly. The age of the failed fuel computed from Cs^{136}/Cs^{137} ratio present in primary sodium confirmed this measurement.

In the recent past, the CG has also started a programme to utilize FBTR for the production of societally beneficial radioisotopes. As a part of this programme, Sr^{89} , a beta emitter used for alleviating pain in bone cancer patients, was produced in FBTR through the irradiation of yttria. CG has demonstrated the separation of Sr^{89} from the irradiated yttria in the hot cells and its subsequent purification by ion-exchange. Characterisation of the Sr^{89} is now in progress, and in the near future, the process know-how would be passed on to the Board of Radiation and Isotope Technology.

CONTRIBUTIONS TO PFBR AND FUTURE FAST REACTORS

Chemical Sensors

The development of electrochemical meters for monitoring hydrogen, carbon and oxygen in sodium has been a major highlight of the contributions of CG. In particular, the development of the Electrochemical Hydrogen Meter (ECHM) to detect water-



Figure 1: Electrochemical hydrogen meter ECHM

steam leak in the steam generator at the incipient stage is one of the excellent contributions from the CG. Several versions of these meters were fabricated and tested for their long term performance in bench top loops as well as in large sodium loops in the Centre, and FBTR. This development had demanded several years of basic studies on various electrolyte systems including their phase diagrams and electrical conductivity measurements. This work has finally resulted in a robust ECHM (Figure 1) that can measure a change in ~ 10 ppb of hydrogen in sodium in a background of around 50 ppb. One hydrogen meter has been installed in the PHENIX reactor in France as a part of the collaboration programme between IGCAR and CEA, and its performance was as good as that of the hydrogen meter based on mass spectrometer. The excellent performance of the ECHM has provided us confidence to introduce the same as the primary steam generator tube leak detection system in the PFBR.

A diffusion based hydrogen detection system has been developed to monitor the hydrogen concentration in the argon cover gas during start up or low power operation of the fast reactor. Four units of this system are now being fabricated for integration in PFBR. An electrochemical meter for the measurement of carbon activity in sodium has also been developed. The activity of carbon measured by this meter has been compared with the data obtained by foil equilibration measurements. From the temperature response of the cell the nature of carbon species in molten sodium was also evaluated. For the measurement of oxygen in sodium, a yttria doped thoria (YDT) solid electrolyte based electrochemical sensor has been developed and is undergoing tests in various loops.

Chemistry Group is also engaged in the development of compact chemical sensors for a wide variety of other applications, besides basic research on sensor materials and sensing processes. Sensors based on thin films of semiconducting oxides (eg. tin oxide) have been developed. Thin film hydrogen sensor based on tin oxide has extended the detection limit of the hydrogen detection system for cover gas (based currently on Thermal Conductivity Detection) down to a few vppm. The sensor has performed satisfactorily in different engineering scale facilities of our Centre for more than five years. Promising semiconducting oxide formulations have also been identified for sensing oxides of nitrogen (NO_x), oxygen, ammonia and hydrogen sulphide. The sensor systems will be useful for the reprocessing plants, reactor operating areas and heavy water production plants.

Cleaning of Sodium Wetted Components

Components exposed to liquid sodium in coolant circuits of fast reactors need to be cleaned free of sodium when removed from coolant circuits for periodic maintenance or replacement. A water vapour-CO₂ process for cleaning sodium from reusable large components has been studied at CG. A pilot plant (Figure 2) was constructed and the sodium cleaning experiments carried out in the pilot plant showed that the cleaning process could be carried out in a controlled manner by manipulating injection of moisture into the reaction chamber. Accordingly, this process has been recommended for cleaning sodium wetted components of PFBR.

Chemical and Electrochemical Decontamination

A chemical decontamination method for primary components of PFBR using sulpho-phosphoric acid was standardized with inactive SS316LN specimens exposed to sodium. The process conditions such as chemical composition of the decontamination solution, temperature and the process time were optimized for various sodium sensitized cold worked specimens. The chemical decontamination formulation, evolved based on these studies has been recommended for decontamination of primary components of PFBR. An electrochemical brush decontamination method was also standardized for decontamination of hot spots of primary components of PFBR using SS316LN material, in collaboration with CECRI, Karaikudi.

Boron Chemistry

One of the important contributions of the Chemistry Group towards PFBR was the development of the technology for the production of elemental boron required for fabricating the absorber rods, in association with BARC and Heavy Water Board (HWB). Figure 3 shows the pilot plant for elemental boron production. The process for the conversion of boric acid to potassium tetrafluoroborate (KBF₄) and its subsequent conversion to elemental boron through molten salt electrowinning route were optimized at the laboratory and the know-how transferred to HWB, which is presently engaged in regular production of elemental boron through this route. During this process, a few kilogram of pure enriched elemental boron was also produced and characterized and the



Figure 2: Pilot plant for sodium wetted component cleaning: water vapour - CO₂ process



Figure 3: Pilot plant for elemental boron production

material was sent to BARC for conversion to boron carbide. The group was responsible for the determination of B^{10}/B^{11} ratios in a large number of samples, generated during the development of the ion-exchange based enrichment process at IGCAR, and the determination of the ratio also in the boron produced at Manuguru as well as boron carbide fabricated at BARC. Experiments to assess the chemical compatibility of high-density boron carbide pellets with D9 clad material in the presence of sodium were also carried out.

The Chemistry Group also set up a unique facility for measuring the isotopic ratio of boron in irradiated boron carbide pellets, using the home built reflectron time of flight mass spectrometry. Using this facility, the analysis of the isotopic ratio of B^{10} to B^{11} in the carbide pellets in the control rod of FBTR that was discharged from the reactor was measured. These data have provided important inputs about the feasibility of recycling of the enriched boron carbide.

Cover Gas Purification System

The cover gas purification system in PFBR uses activated charcoal at cryogenic temperatures to delay the passage of radioactive isotopes of krypton and xenon which ensures that they decay considerably before they are let out into the atmosphere. In collaboration with FRTG, CG has carried out the demonstration of the cover gas purification system on a pilot plant scale. The dynamic adsorption coefficient of charcoal for krypton and xenon was measured and the data have been used to arrive at the amount of charcoal required for the purification for PFBR.

FAST REACTOR FUEL CYCLE

In the Indian context, the fuel cycle of fast reactors pose many unique challenges. The first Indian experience of fast reactors was with high plutonium content mixed carbide fuel for FBTR; the PFBR would use mixed oxide fuel, while future fast reactors are expected to use metal alloys as the fuels. Thus, the group has engaged itself in the study of all these fuel systems as well as their fuel cycle aspects. In the recent past, the CG has been playing a key role in the development of fabrication routes for fuel



Figure 4: Spot technique for measurement of solidus-liquidus temperature of fuel materials

materials and also fabrication of test fuel pins in collaboration with BARC.

Fuel Chemistry

Chemistry Group has carried out thermophysical and thermochemical property measurements of a variety of fuel materials, fission product systems and compounds of alkali metals. Heat capacity and thermal conductivity data of U-Pu mixed oxides, carbides and nitrides, as well as oxygen potential over mixed oxide have been measured in the Chemistry Group. More recently, the novel "SPOT technique" (Figure 4) was established for the first time to measure the solidus liquidus temperatures of fuel materials. The U-Zr system was comprehensively studied using this technique. Efforts are now on to make measurements on the carbide fuel of FBTR and metal alloy systems.

Fuel Cycle Chemistry

In collaboration with BARC, CG has set up a unique lab scale facility for the fabrication of test fuel pins using fuel materials synthesized through SOL-GEL route. The fabrication of test fuel pins with $(U_{0.6}Pu_{0.4})$ mixed oxide is being pursued and the test fuel pins will be introduced in FBTR for irradiation in the coming months. The group has also demonstrated lab scale synthesis of U-Pu mixed oxide microspheres with 28% Pu, and U-Am mixed oxide microspheres with 5% Am.

Extensive investigations were carried out on the extraction of actinides by tri-n-butyl phosphate (TBP) extractant used in the PUREX process for reprocessing and also other members of trialkyl phosphate family. A thorough investigation on the phenomenon of third phase formation in the extraction of plutonium by TBP generated the understanding that was vital in the design of the process flow sheet in the reprocessing of fast reactor fuels. To avoid the possibility of third phase formation, several other trialkyl phosphates and especially tri-isoamyl phosphate (TiAP) were investigated. Counter current liquid-liquid extraction experiment, carried out with TiAP solvent under the conditions simulating the PUREX process, has indicated satisfactory behaviour of the TiAP.

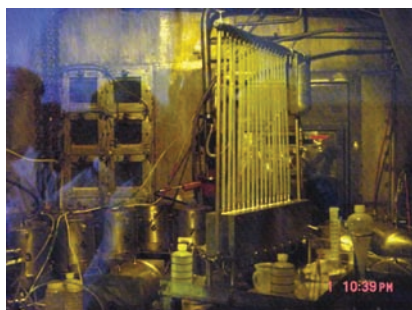


Figure 5: The setup used for minor actinide partitioning in hot cell



Figure 6: Mixer-settler facility used for flow sheet development studies with TiAP for fast reactor fuel reprocessing

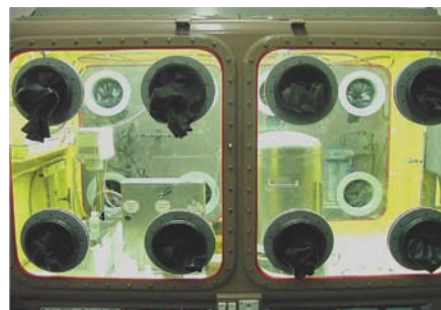


Figure 7: Supercritical fluid extraction facility in glove box for recovery of actinides from waste matrices

The Chemistry Group has also been active in the area of minor actinide partitioning (Figure 5) from high-level liquid waste. The group has synthesized the extractant octyl(phenyl)-N,N-diisobutyl carbamoyl methyl phosphine oxide (O Φ CMPO) and carried out several extraction experiments with americium and other lanthanides such as neodymium. Recently, a typical high active waste arising from the reprocessing of the carbide fuel of FBTR irradiated to a burn-up of 155 GWD/Te was transported from the CORAL facility to RCL. A mixer settler run was carried out in the hot cells of RCL using the CMPO extractant, which established the recovery of over 99% of the minor actinides (Figure 6). For this experiment, CG developed a complex formulation that enabled the stripping of the actinides and lanthanides without the formation of interfacial crud. The group has also synthesized novel and unsymmetrical diglycolamide and diglycolamic acid extractants. The extraction data on various solvent systems generated will be very useful for arriving at a partitioning scheme for the minor actinides from the high-level waste generated in fast reactor plants.

Development of Glass and Ceramic Matrices for Radioactive Waste Immobilization

Borosilicate glass is the accepted matrix world over, for the immobilization of the high-level radioactive liquid waste generated in nuclear fuel reprocessing. However, this matrix may have many limitations for the immobilization of high-level liquid waste from fast reactor fuel cycle. Chemistry Group has been carrying out a systematic study on alternate matrices to address this issue. Iron phosphate glass and crystalline synthetic rock (synroc) are examples of matrices that have been explored. Simulated waste forms based on these two have been fabricated, and their thermophysical and thermochemical properties have been studied using a number of techniques. The matrices have also been subjected to rigorous chemical durability studies in order to evaluate their potential.

Advanced Separations

The Chemistry Group has also made several original contributions

in the development of a variety of advanced separation techniques. The group has demonstrated high resolution, fast separation of individual lanthanides and actinides based on high-level liquid chromatography. In fact, CG was the first to demonstrate rapid separation of all the lanthanides using small particle columns and monolith columns. A separation time of 2.7 minutes for all the fourteen lanthanides achieved by the Chemistry Group is, as of now, the shortest reported in liquid chromatographic separation of the lanthanides. These techniques have been very valuable for the determination of the burn-up of FBTR fuel with considerable reduction in analysis time and consequent reduction in the radiation dose to the operator.

The Chemistry Group has also set up for the first time, a supercritical fluid extraction facility (Figure 7) inside the glove box for recovery of actinides from various waste matrices and was the first to demonstrate quantitative recovery of uranium, plutonium and americium from tissue waste, and a novel modifier free approach for application to systems where the extractant is a solid. The extraction procedure developed was demonstrated on actual waste generated in the fuel cycle operation.

The Chemistry Group has also carried out pioneering work on the applications of room temperature ionic liquids (RTIL) for actinide and fission product separations. The use of RTILs as a diluents, extractant and electrolytic medium has been investigated. The Chemistry Group was the first to demonstrate the extraction and electrodeposition technique for the recovery of uranium and palladium from nitric acid medium. The electrowinning of uranium oxide by oxidative chlorination of the oxide to chloride form in ionic liquid medium followed by electrodeposition as oxide was also demonstrated.

Fuel Cycle for Metal Alloy Fuelled Fast Reactors

Metallic fuels will be introduced in future commercial fast reactors in India to exploit their high breeding potential and enhance the growth of fast reactors in the country. Towards the development of the front end of the metal fuel cycle, IGCAR has taken up a programme in close collaboration with BARC to fabricate sodium



Figure 8: Glove box train facility for sodium bonded metallic test fuel pin fabrication

bonded and mechanically bonded test fuel pins and irradiate them in FBTR. A lab scale facility for fabrication of test fuel pins with sodium bonding has been set up by the Chemistry Group (Figure 8). U-Zr alloy slugs supplied by BARC have been encapsulated in the pins and currently six of these pins are now being irradiated in FBTR. It is now planned to take up fabrication of test fuel pin containing enriched U-Zr alloy and subsequently U-Pu-Zr alloy.

Unlike the oxide and carbide fuels that are processed by the conventional PUREX process, the metallic fuel will be processed by pyroelectrochemical route. CG has been engaged in the R&D of pyrochemical processing of metal fuels for nearly two decades. Starting with a lab scale facility, in which electro-refining of uranium was demonstrated on 200 gram scale, an engineering scale demonstration facility (Figure 9) for process studies on a one kilogram scale has been commissioned. Electrorefining experiments have been carried out on kilogram scale with U metal as well as U-6%Zr alloy. Studies on the electrorefining of plutonium and its rare earth alloys on lab scale to understand the chemical behaviour before scaling up the process were carried out. The group is now engaged in setting up facilities, along with Fast Reactor Technology Group, for electrorefining and consolidation studies on ten kilogram scale. Several studies have been taken up on a fundamental plane on molten salt chemistry and thermochemistry relating to pyroprocessing. Studies on electrochemical reduction behavior of plutonium and zirconium ions in LiCl-KCl molten salt at various temperatures have been carried out by transient electrochemical techniques such as cyclic voltammetry and chronopotentiometry. Towards modelling the electrorefining process, a code, based on thermochemical equilibria (PRAGAMAN) and a code based on diffusion layer theory (DIFAC) have been developed.

Direct Electrochemical Reduction of Uranium Oxides

Currently, the actinide metals are produced by the calciothermic reduction of their respective fluorides which in turn are produced from their oxides. The direct electrochemical reduction of uranium oxides by making them as the cathode of an electrolytic



a)



b)

Figure 9: a) Engineering scale demonstration facility for pyroprocess studies on uranium alloys and b) uranium metal ingot consolidated from electrorefining

cell using platinum/graphite as anode and the molten salt LiCl or CaCl₂ containing small amounts of lithium oxide or calcium oxide as the electrolyte has been studied, and efforts are on to optimize the process parameters to achieve complete reduction and extend the process for PuO₂.

BASIC RESEARCH

Thermochemistry

The Chemistry Group has pursued a number of programmes in basic research related to the mission programmes. High temperature mass spectroscopy has been an area of specialization in Chemistry Group. Using the Knudsen mass spectrometer established for the first time in the country, a large number of systems of relevance to fuel cycle interaction in oxide fuels such as tellurides of iron, nickel and chromium have been studied. Phase diagrams and vaporization behaviour have been established for the first time in several systems. The thermal expansion behavior of (U,RE) mixed oxides as well as the solubility limits of rare earth oxides were also determined using high temperature X-ray diffraction. The heat capacity data of these mixed oxides by differential scanning calorimetry have also corroborated the solubility limits of rare earth oxides.

Separation Science

Third phase formation during the extraction of Th(IV) and Pu(IV) by several trialkyl phosphates such as TBP, tri-iso-butyl phosphate (TiBP), tri-sec-butyl phosphate (TsBP), TAP, T2MBP, TsAP etc., were studied in a comprehensive manner. Studies have also been carried out on third phase formation in the extraction of trivalent lanthanides by CMPO based solvents. A number of phosphonate extractants such as Dibutylbutyl phosphonate (DBBP), Dibutylhexyl phosphonate (DBHeP), Dibutyloctyl phosphonate (DBOP) and Diamylamyl phosphonate (DAAP) have been synthesized and studies on extraction of actinides (U, Th, Pu and Am) and third phase formation have been carried out in detail for the first time. A unique instrument has been developed for the measurement of phase separation time of solvents based on light scattering technique. The thermal decomposition of TBP-

nitric acid systems was also studied by adiabatic calorimetry. Enthalpy and activation energy of decomposition of nitric acid solvated TBP were reported for the first time.

A laser mass spectrometry system comprising in-house developed reflectron time-of-flight mass spectrometer was used to study solid and liquid samples containing UO_2 doped with lighter rare earths, towards developing a method for the direct determination of burn-up of irradiated nuclear fuel, without chemical separations on the fuel solution.

Boron Chemistry

Besides demonstrating the production of enriched elemental boron, a number of basic studies on the electrochemistry of boron in the molten salt medium as well as vaporization chemistry of boric acid were carried out. The vaporization behavior of $H_3BO_3(s)$ was studied by the transpiration method (using a commercial thermo gravimetric apparatus) as well as Knudsen Effusion Mass Spectrometry (KEMS). Using Ag/AgCl reference electrode developed in-house, for the first time, the cyclic voltammogram of boron deposition on a platinum electrode from $KCl-KF-KBF_4$ molten salt mixture was recorded. The influence of oxide-ion impurity in the $KCl-KF-KBF_4$ melt system on the electrode potentials was also investigated by linear sweep voltammetry.

Matrix Isolation Infrared Spectroscopy

A Matrix Isolation – Fourier Transform Infrared Spectroscopy facility (MI-FTIR) has been set up to study the conformations of organic molecules and intermolecular interaction between the molecules. Using this facility, conformations and structures of trimethyl phosphate, triethyl phosphates, tributyl phosphate, phosphites, phosphonates, methoxy compounds, carbonates and silanes were studied. By controlled annealing experiments, weak and strong hydrogen bonded complexes and van der Waals complexes have also been studied. CG is now in the process of setting up a MI-FTIR facility at RRCAT, Indore to carry out photochemical studies on some of the systems indicated above, using the Synchrotron facility.

Fluorescence Spectroscopy

Fluorimetric methods were developed to detect uranium and lanthanide ions such as terbium, dysprosium, europium, and samarium at trace levels ($<10^{-8}$ molar) using the method of ligand sensitized fluorescence. Various methods of fluorescence enhancement such as the use of synergic ligands and addition of other “acceptor” ions were investigated. Using co-fluorescence, an enhancement of four orders of magnitude in fluorescence of uranyl ion has been noticed in presence of yttrium ion and trimesic acid as ligand.

Development of Radionuclide Trap Materials for Liquid Sodium

CG has been engaged also in the development of radionuclide traps (RNT) for various radioactive species in liquid sodium

coolant. In the recent years, an in-house synthesized low density porous carbon foam (HMPC) was used for demonstrating the efficient removal of cesium. Efforts are in progress to increase the porosity and to increase the extent of graphitization of HMPC for use as effective trap material for cesium isotopes.

GENERAL

The Chemistry Group has also established a good network of collaboration with various academic and research institutions in the country. Collaborations have also been pursued with CEA, France in the areas of sodium chemistry and thermochemical modeling of mixed oxide actinide systems.

The success of CG can be attributed to the multidisciplinary strengths available in the group. Thus, besides taking up various basic research activities in chemistry related to the fast reactor programme, the group has in fact developed many processes on pilot plant scale and also developed products that are available for direct utilization in the programme. For this purpose, CG has focused on the development of an in-house engineering strength with regard to chemical facilities as well as instrumentation. The engineering scale experiments on pyrochemical reprocessing, the fabrication of sodium bonded fuel pins and the mixer settler runs in the hot cells are examples that illustrate the comprehensive capabilities in chemistry, chemical engineering, instrumentation and other allied disciplines that have been built in Chemistry Group. The analytical instruments used in the CG have been upgraded / retrofitted by incorporating modern data processing systems and software. The CG has in its fold, a number of old characterization facilities that have been kept functional through in-house maintenance and upgradation.

As the major chemistry laboratory in the Centre, the group has continued to provide excellent analytical support to a number of programmes of the centre besides meeting its own requirements. In the last five years, the analytical capabilities have been further fine tuned by adopting the ISO certification. A number of new analytical procedures have also been developed especially in the context of boron production. The group has also been playing a catalytic role in the dissemination of information regarding radioactivity and radioisotopes through several workshops in schools and colleges.

The Chemistry Group has played a pivotal role in the fast reactor programme, addressing various current issues as well as taking up challenging and innovative programmes that would enable it to remain poised for solving any chemistry issue that may be faced in future development of the fast reactor programme.



S. C. Chetal
Director, IGCAR

Performance Testing of Primary Ramp and Primary Tilting Mechanism of Inclined Fuel Transfer Machine of Prototype Fast Breeder Reactor

Prototype Fast Breeder Reactor employs two machines for handling fuel sub-assemblies within and out of the main vessel, viz. (i) transfer arm – for in-vessel handling of fuel, blanket and control sub-assemblies within the main vessel and (ii) inclined fuel transfer machine – for transfer of spent sub-assemblies out of the main vessel and replacing them with fresh sub-assemblies (Figure 1). The primary side of the inclined fuel transfer machine consists of: primary tilting mechanism, primary ramp, shield plug, inter connecting piece, bellows and primary gate valve. Primary tilting mechanism is bolted to the grid plate and primary ramp is located on the primary ramp liner of roof slab. The bottom of the primary ramp engages with the guide funnel of the primary tilting mechanism to form a sliding joint that accommodates the differential thermal expansion between primary ramp and primary tilting mechanism from room temperature to various operating conditions (normal operation/ fuel handling). The secondary side of the inclined fuel transfer machine consists of secondary gate valve, secondary ramp and secondary tilting mechanism, which are located inside the fuel building. Primary side and secondary side of inclined fuel transfer machine are interconnected through the rotatable shield leg, which includes a rotatable table supported on a slewing ring. During fuel handling, the spent fuel sub-assembly is loaded into the transfer pot, which is inside primary tilting mechanism

by transfer arm. Transfer pot containing the sub-assembly and sodium to remove decay heat from the spent sub-assembly is hoisted through primary ramp into rotatable shield leg which then rotates by 180° to engage with secondary side. Transfer pot with sub-assembly is then lowered into the secondary tilting mechanism thus transferring the spent sub-assembly from the in-vessel transfer position located in the periphery of the core to the ex-vessel transfer position located in fuel building. The transfer pot is then loaded with a fresh sub-assembly and the above sequence of operations is then reversed to transfer a fresh sub-assembly back into the reactor.

Two tilting rails and one guide rail are provided on both the primary and secondary sides of inclined fuel transfer machine and corresponding tilting and guide rollers are provided on the transfer pot. The rollers are high temperature ball bearings designed to work in sodium. Material selection of rollers and hard facing of the rails is based on tribological considerations suitable for sodium service. Rails of primary/secondary tilting mechanism are designed such that transfer pot is tilted from 17° 23' inclination to vertical while lowering in them and vice-versa.

Primary ramp and primary tilting mechanism (Figure 2) were fabricated by M/s MTAR, Hyderabad. After completion of shop

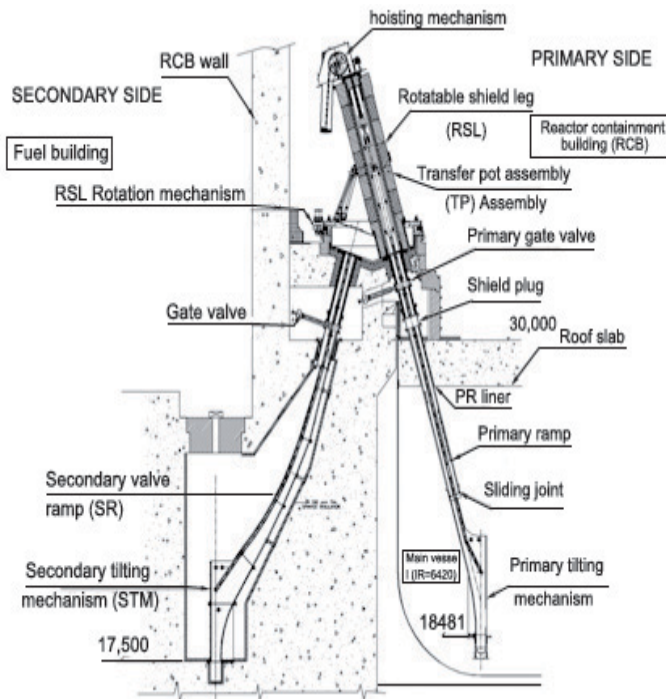


Figure 1: Inclined fuel transfer machine

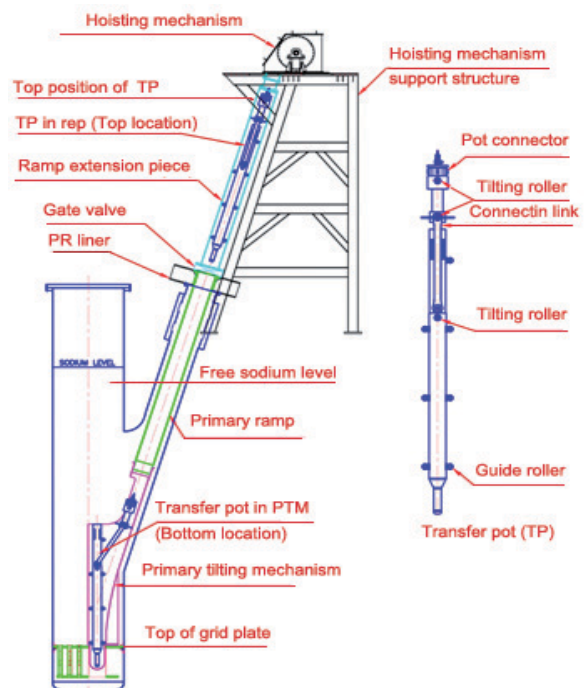


Figure 2: Schematic of primary ramp/primary tilting mechanism test set-up



Figure 3: Primary ramp with primary ramp liner



Figure 4: Ramp extension piece, drive mechanism and support structure

floor testing, performance testing was carried out in test vessel-2 of the large component test rig under reactor simulated conditions. The testing was limited to ~10 % of the total number of cycles expected in the reactor life of 40 years as the same components are to be installed in the reactor after testing.

Primary ramp and primary tilting mechanism were assembled in test vessel-2 of large component test rig along with additional components like ramp extension piece, gate valve, simplified hoisting system with support structure and transfer pot with dummy sub-assembly. Schematic of test set-up is shown in Figure 2. Test vessel-2 is a vessel of 2 meter diameter and 12 meter height. It is provided with a branch pipe at 17° inclination to simulate the assembly of primary side of inclined fuel transfer machine. Primary tilting mechanism was bolted to the grid plate inside test vessel-2 while primary ramp was mounted on a specially fabricated liner simulating the rigid support in the reactor (Figure 3). The entire length of primary ramp was housed in the branch pipe at 17° inclination to vertical. Relative motion between primary ramp and primary ramp liner was arrested by two locking pins. Transfer pot with dummy sub-assembly was lowered into the primary tilting mechanism through primary ramp followed by sequential assembly of gate valve and ramp extension piece (Figure 4). The top of ramp extension piece was connected to the structure supporting the hoisting mechanism through another sliding joint with O-ring sealing. The assembly of the primary ramp, primary tilting mechanism and ramp extension piece was carried out such that inclination of 17° to vertical of primary ramp, ramp extension piece and alignments of the rails were achieved. The alignment of guide rails between primary ramp and primary tilting mechanism was critical and was achieved within 0.5 mm. The hoisting mechanism consists of chain and sprocket arrangement, sprocket shaft, motor (3.7 kW, 1440 RPM) with

brake and speed reduction gear train (helical gears with worm reducer, reduction ratio of 1000:1). A torque limiting safety coupling is provided between the motor and driving end of gear train. The sprocket and sprocket shaft are housed inside a leak tight housing with viewing windows. Operation of the test set-up was carried out through a control console incorporated with safety interlocks.

The instrumentation provided for the hoisting mechanism includes continuous on-line monitoring of transfer pot position using potentiometer, automatic stop of transfer pot at top limit using reed switch and potentiometer, and at bottom limit using tension sensing mechanism, potentiometer, and limit switches to identify open and closed positions of gate valve. In addition to the above, thermocouples are provided at various locations along the vessel, branch pipe and ramp extension piece to monitor temperature. An arrangement consisting of dial gauges and linear variable differential transformer is provided to monitor the deflection of test vessel-2 at the elevation of the grid plate during high temperature operation.

One cycle of testing consisted of the following operations:

- Hoisting of transfer pot with dummy sub-assembly from inside primary tilting mechanism at 29.2 mm/s speed (corresponds to motor speed of 600 RPM) from bottom position i.e. 22400 to 24279 mm elevation
- Hoisting through sliding joint between primary ramp and primary tilting mechanism at 7.3 mm/s speed (corresponds to motor speed of 150 RPM) up to 29550 mm elevation
- Hoisting inside primary ramp at 29.2 mm/s speed up to 29550 mm elevation
- Hoisting at gate valve location at the speed of 7.3 mm/s up to 31400 mm elevation
- Hoisting inside ramp extension piece at 29.2 mm/s speed up to topmost location i.e. 35800 mm elevation. During hoisting, transfer pot was parked for 150 s at 29660 and 32405 mm elevations respectively for siphoning and dripping of sodium from it
- Lowering of transfer pot from top most elevation to bottom elevation with different speeds at different elevation as mentioned above

Elevation details of primary ramp/primary tilting mechanism test set-up for set value and observed value during testing are given in Table-1.

Performance testing of primary ramp and primary tilting mechanism was carried out in various stages viz. in air at room temperature, in hot air and in sodium at 200°C which is the fuel handling temperature of Prototype Fast Breeder Reactor. The

Table-1: Elevation details of primary ramp/primary tilting mechanism test set-up

Position of transfer pot	Set point	Raising	Lowering
Top	35800	stop by potentiometer signal	manual start at 600 RPM
Dripping	32045	stop 150s for dripping	NA
Speed change-3	31400	speed to 600 RPM	speed to 150 RPM
Speed change-2	29550	speed to 150 RPM	speed to 600 RPM
Speed change-1	24279	speed to 600 RPM	speed to 150 RPM
Bottom	22400	manual start at 150 RPM	stop by potentiometer signal

performance of the system was monitored continuously by measuring the current drawn by motor (measure of motor torque) and monitoring the system for noise and vibration. A total of 100 cycles of air testing was carried out at room temperature. Current drawn by the motor was within 4.4 A. Measured value of torque was within 15 to 16 N-m. No rubbing marks or scoring marks were observed on the rails and rollers. Overall performance of the system was satisfactory.

In order to conduct sodium tests, pressure hold test of the system was conducted for 24 hours duration with compressed air at a pressure of 200 mbar (g). Hot purging was done which reduced the moisture and oxygen levels in the system to 118 and 487 vppm, respectively. Prior to the start of sodium tests, hot air test was carried out for 24 cycles at different temperatures of 65, 95, 110, 125 and 150°C. Overall performance of the system was satisfactory. Current drawn by the motor and torque values were well within the acceptable limits.

In sodium performance testing was carried out at 200°C. Oxygen level in sodium was maintained to less than 2 ppm. The effect of reactor operation at rated temperature of 547°C on the aerosol deposition in cold regions like gate valve was also simulated by means of two dwell period tests each of 150 hours duration at 547°C. The dwell periods were interspersed between the cyclic tests. The system was tested for a total of 510 cycles in sodium. The performance of the system was along expected lines. Maximum current drawn by the motor was within 4.5 A. Measured values of torque were within 14 to 19 N-m.

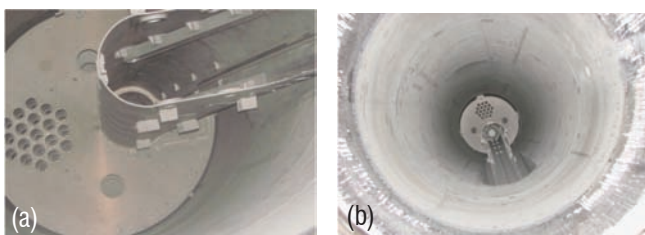


Figure 5: Primary tilting mechanism inside the test vessel a) before reaction and b) after reaction

After completion of the testing, the sodium in test vessel-2 was drained and vessel cooled to 60°C. Test vessel-2 was isolated from large component test rig loop and connected to a specially fabricated system for sodium removal using water vapor-CO₂ process. The cleaning process was very effective (Figure 5). A total of 3 kg of sodium was removed by this method. The value obtained experimentally (from H₂ monitoring during the process) was close to that obtained by estimation. The time taken for vapor phase reaction was 85 hours. The vapor phase reaction was followed by water wash using fine spray followed by washing in distilled water in a jet facility erected for the purpose as well as in a specially fabricated water tub. The rollers of transfer pot were dismantled and cleaned in ultrasonic bath.

After cleaning and drying, primary ramp and primary tilting mechanism were inspected by Quality Assurance Division. Visual examination of the primary ramp and primary tilting mechanism revealed no scoring or rubbing marks on the rails. The weld between the primary tilting mechanism body and base plate was subjected to liquid penetrant inspection examination and found to be defect free. Liquid penetrant inspection examination of accessible portion of the primary ramp and primary tilting mechanism rails indicated absence of cracks. All screws holding the rails of primary tilting mechanism and primary ramp to the body were tack welded and the components cleaned by acetone, packed and dispatched to BHAVINI.

The successful completion of the performance testing of primary ramp, primary tilting mechanism in air and sodium, and the effective *in situ* removal of sodium from primary ramp and primary tilting mechanism by water vapor and CO₂ process have qualified the component for reactor operations. Visual examination followed by the subsequent liquid penetrant inspection examination of components after cleaning has confirmed the healthiness of the components.

Reported by B.K.Sreedhar, Fast Reactor Technology Group and S.Raghupathy, Reactor Design Group

Science of Metal Nanoclusters

Now it may be the time we say goodbye to the well-known old proverb: Big is Beautiful. Almost everyday the world is witnessing advancement and breakthrough discoveries that lead to miniaturization of devices through the knowledge of nanoscience and nanotechnology. 'Nano' is a generic buzz-word in this context. As we know, nanomaterials are nothing different from the parent phase of materials except its' physical dimension ranges between 1-100 nm ($1\text{ nm}=10^{-9}\text{ m}$), at least in one direction. At the nanoscale, physical, chemical and biological properties of materials differ from the properties of individual atoms and molecules or bulk matter. That brings up spiraling applications of various nanoscale materials in almost every sphere of life. So, understanding the science of synthesis and novel properties of matters at nanoscales is one of the most active areas of research today. It brings out abundance of unexpected results to ponder. In this perspective, metal nanoclusters that form an important class in the world of nanomaterials may deserve special attention for a comprehensive research study. Metal nanoclusters may be synthesized as embedded in various matrices or supported on functional substrates of interest. Synthesis of metal nanoclusters and nanostructures has been broadly classified according to two approaches: bottom up and top down. As the name suggests, the first method deals with techniques where nanoclusters are grown from single atom onwards. Top down approaches start exactly in the reverse way: from bulky crystals to nanocrystals of nanoclusters. Thus, there are some successful techniques for the processing of such novel materials, for example, metal dielectric co-sputtering, recoil-implantation, molten salt bath, direct implantation of metal ions, sol-gel, evaporation-condensation, electron beam lithography, optical lithography, ion-beam induced sputtering, etc. Controlled synthesis of size-selective metal nanoclusters in various media is of prime importance as most of the exotic properties depend primarily on their physical dimensions. To realize a better control on the preparations, basic understanding of the mechanisms governing formation and evolution of metal nanoclusters while processing these novel materials is of great interest.

Rich phenomena such as strong optical responses in the ultraviolet-visible to near infrared wavelength ranges of light, photoluminescence, local field enhancements, etc. are associated with metal nanoclusters and nanostructures. Interaction of visible light with surface electrons of metal nanoclusters, for example, leads to fascinating colors of glasses through an optical phenomenon (known as surface-plasmon resonance). Colors of the glass depend on size, shape and number density of the metal nanoclusters as well as on dielectric constants of the media. In addition, this optical effect leads to large local field enhancements in the close vicinity of metal nanoclusters. These novel physical

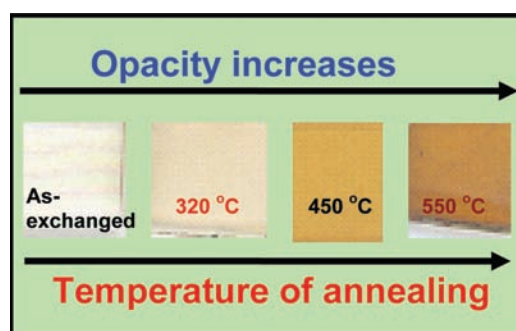


Figure 1: Photographic image shows the change of optical features of the silver-exchanged soda-glass samples due to the isochronal heat treatments

effects have been motivating fundamental and experimental researchers for a long time extensively. Such research driven challenging applications of the plasmonic nanostructures are numerous. For example, fast-response optical switches, high sensitivity nanosensors, information storages, chemical catalysis, tumor or cancer diagnosis and treatments, surface-enhanced Raman spectroscopy, solar cell materials and so on. Accordingly, besides their exciting scientific and technological interests, research studies of nanoscale materials are becoming highly relevant in diverse disciplines including biology and medicines. However, there are several difficulties in handling, detection and measurements of such tiny materials due to their physical restrictions.

Embedded Metal Nanoclusters in Glass Matrices

Nanoscale silver clusters have been prepared in a soda-glass matrix through the silver ion-exchange ($\text{Ag}^+ \leftrightarrow \text{Na}^+$) process. Ion-exchange of various metal ions in soda glasses followed by thermal annealing or light ion irradiations (H^+ , He^+) are methods to modify linear and nonlinear optical properties of glasses. The method is commercially viable for applications in optoelectronic devices. Due to the technological importance, precise spectroscopic studies to elucidate the thermal stability of these optical nanomaterials are of great interest. A simple photograph is shown in Figure 1 to demonstrate how the colors have changed due to the given heat treatments. As seen, with the increase of annealing temperature, samples have darkened significantly. Darkening, or in other words, increase in the opacity implies that optical absorption density has increased consistently with the annealing temperature. This qualitative visual observation conforms to the precise experimental results of optical absorption spectroscopy (Figure 2b). Metal nanoclusters are experimentally identified through the characteristic optical resonance (surface-plasmon resonance) wavelengths. In case of Ag nanoclusters in a glass matrix, surface-plasmon resonance position is $\sim 420\text{ nm}$.

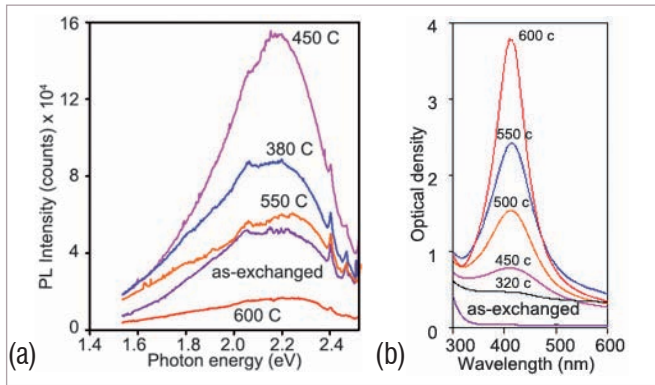


Figure 2: (a) Photoluminescence (with 488 nm excitation) and (b) optical absorption spectroscopy of Ag nanoclusters in the matrix

Increase in the absorption intensity with the increase of annealing temperature is attributed to the thermal growth of the silver nanoclusters in the glass matrix. The observed growth may be explained from Mie theory of light scattering. Assuming average size of metal nanoclusters to be much smaller than the optical wavelength, Mie theory calculates the resonance absorption intensity to scale up with volume fractions of metal nanoclusters. Photoluminescence spectroscopy results corroborate further with the growth of the silver nanoclusters. For example, drastic changes in the photoluminescence intensity have been observed on post-annealing the silver-exchanged glass samples at various temperatures (Figure 2a). Silver monoxide (Ag_2O) formed in the as-exchanged soda-glass sample is chemically unstable and it decomposes into species like Ag_2O and Ag while annealing in vacuum around 380°C . Further increase of annealing temperature only helps in the growth of the Ag nanoclusters due to thermal decomposition of Ag_2O . As a result, the photoluminescence intensity quenches (Figure 2a). A strong correlation of the growth of the silver nanoclusters and drastic changes in the photoluminescence intensity due to thermal annealing of the silver-exchanged glass samples has been so established.

Rutherford backscattering experiments have been carried out in these samples to measure the concentration profiles of Ag after thermal annealing (1 hour isochronal) at various temperatures. An analyzing beam of He^+ ions at energy of 2 MeV, backscattered by an angle of 160° , was used during the backscattering measurements. It is observed from the backscattering spectra (Figure 3) that silver got accumulated near the surface of the glass during the annealing. Accumulation of silver is higher for samples annealed at higher temperatures. Near-surface (within ~ 100 nm) accumulation is due to the thermal diffusion of silver ions in the soda-glass matrix. This outward diffusion of silver ions relaxes the stress (which arises due to size difference of Ag^+ and Na^+ ions) and minimizes the total energy in the system. Applying suitable diffusion theory to the Rutherford backscattering data, it has been possible to estimate activation energy for thermal

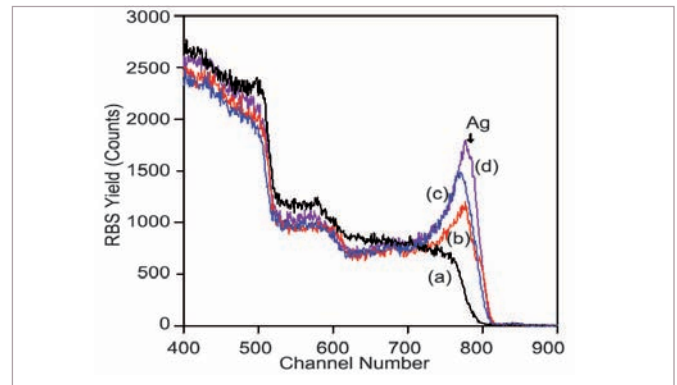


Figure 3: Rutherford backscattering spectra of silver-exchanged soda-glass samples annealed at (a) 320, (b) 450, (c) 550 and (d) 600°C

diffusion of silver ions in the soda-glass matrix. This short-range accumulation of silver ions during annealing allows to consider the case as a semi-infinite diffusion system with the bulk acting as a constant source of known density (say, c_0). Accumulated mass of silver per unit area (m) on the surface can be calculated as, $m = c_0 \sqrt{Dt/\pi}$ where t is the time of diffusion in the sample held at temperature T ; D is the diffusion coefficient of silver ions at temperature T . Assuming D to vary as $e^{-\frac{\epsilon_a}{kT}}$ (ϵ_a is the activation energy for the diffusion of silver ions and k is the Boltzmann constant), m can be rewritten as,

$$\ln(m) = K_1 - \frac{\epsilon_a}{2kT} \quad (1)$$

where K_1 is a constant in the present experimental conditions. For samples annealed at different temperatures, m has been estimated using the expression $m = N_A M / N_{\text{Avo}}$ where N_A (number of Ag atoms/ cm^2) is directly obtained from the backscattering data, M is the atomic weight of silver and N_{Avo} is the Avogadro number. Plugging the Rutherford backscattering data in equation (1), the Arrhenius plot is reported. From the slope of the fitted line, activation energy for the diffusion of silver ions in the soda-glass is estimated to be about 0.74 eV.

Apart from the chemical routes, ion implantation has been a very popular technique to synthesize metal nanoclusters in various matrices. In general, ion implantation techniques provide distinct advantages over many other synthetic processes, because: embedded species are protected by the matrix and hence chemically clean, superior control over depth as well as size distributions and the process is not limited by the solubility factor of the matrix. As the first example, nanoscale cobalt clusters have been synthesized in a silica glass matrix by implanting high energy (2 MeV) cobalt ions. Optical and vibrational properties of the cobalt nanoclusters are particularly interesting. Surface-confined acoustic vibration modes (phonons) of these cobalt nanoclusters have been detected using the low-frequency Raman scattering spectroscopy. Raman scattering spectroscopy

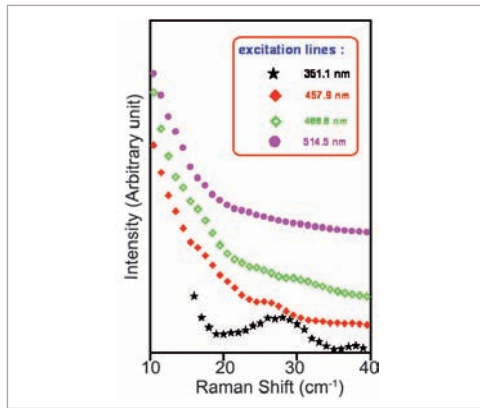


Figure 4: Raman scattering intensity of surface acoustic vibrational modes confined to cobalt nanoclusters as a function of excitation wavelengths (spectra are offset along the intensity-axis for better clarity)

has been used extensively and effectively as a nondestructive experimental means to study the ion implantation-induced growth as well as the thermal growth of the metal nanoclusters in various glass matrices. As shown in Figure 4, Raman spectra have been recorded in the cobalt implanted silica sample using different excitation wavelengths. Interestingly, intensity of the vibrational modes is found to depend significantly on the wavelength of laser excitations (Figure 4). Strong local field of surface-plasmon resonance in cobalt nanoclusters with 351.1 nm excitation wavelength is thought to be the reason for the observed enhancement of Raman scattering intensity. It is because the characteristic surface-plasmon resonance wavelength of cobalt nanoclusters in silica is around 350 nm. Results thus obtained from the Raman scattering spectroscopy experiments, particularly, emphasizes the importance of plasmon-phonon coupling in the metallic nanoclusters.

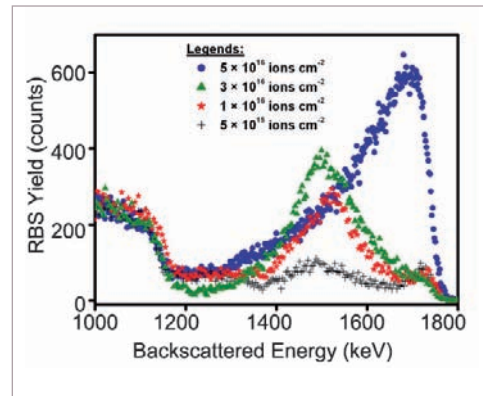


Figure 5: Rutherford backscattering spectra for silver ion implanted soda-glass samples with various ion fluences (indicated with symbols)

In a similar way, using the ion implantation (1 MeV Ag⁺ ions) technique, growth of embedded nanoscale silver clusters in a soda-glass matrix has been studied mainly to highlight interesting optical properties of large scale metal nanoclusters. Prior to the discussion on the optical results, information about concentration profiles of silver atoms in the soda-glass samples measured by the backscattering spectrometry (Figure 5) would be more important. Only the partial spectra at high energy channels are shown here to emphasize the backscattering from silver atoms. Interestingly, in the sample implanted with the highest fluences, most of the concentration of the silver atoms is found to be close to the glass surface (Figure 5, blue dots) and the atomic concentration of silver reduces continuously along the depth in the soda-glass matrix. Defect-enhanced diffusion of Ag atoms in the soda-glass matrix would lead to the segregation of the Ag atoms close to the glass surface. Surface segregation of the Ag

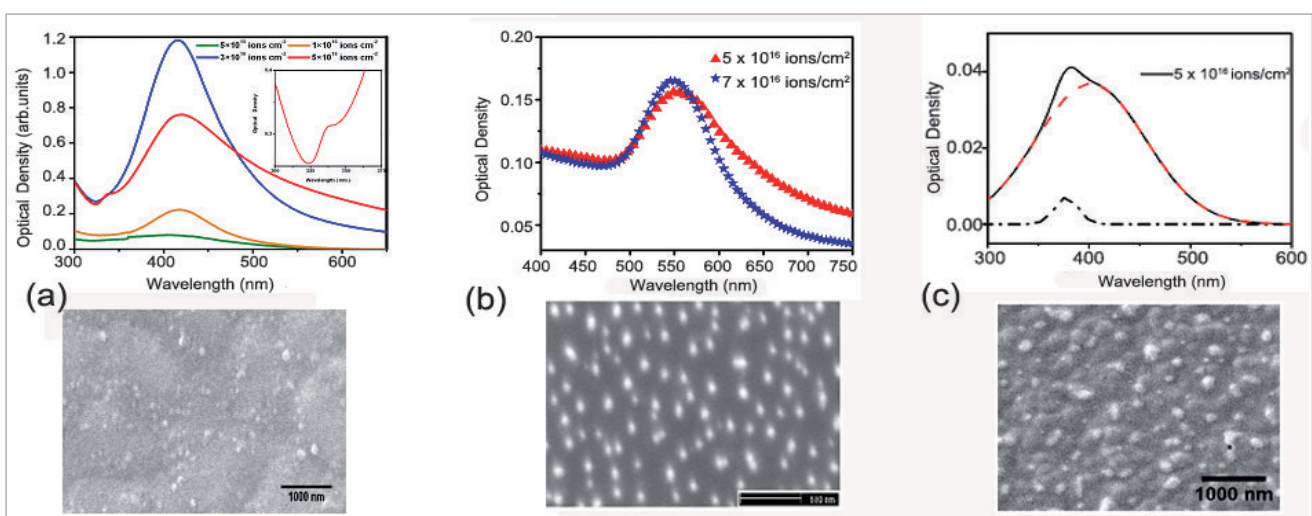


Figure 6: Ag⁺ ion implanted soda-glass sample with fluences 5×10^{16} ions cm^{-2} (Figure a) and ion-beam sputtered (5×10^{16} Ar⁺ ions cm^{-2}) thin film of Ag metals on silica glass (Figure c) show dipolar as well as quadrupolar surface-plasmon resonance absorption in samples with larger Ag nanoclusters. Only dipolar absorption has been observed for Au thin films sputtered with Ar⁺ ions (5×10^{16} ions cm^{-2}) (Figure b). Corresponding scanning electron micrographs display morphologies and various sizes of the Ag and supported Au nanoclusters on the glass substrates.

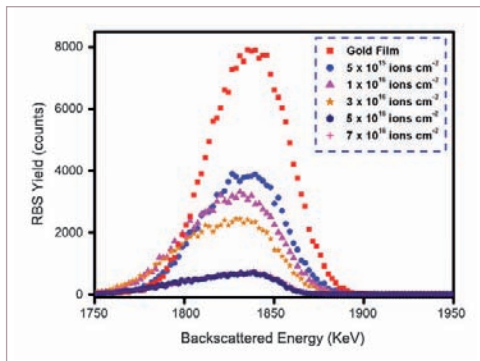


Figure 7: Rutherford backscattering spectra of the Au film and Ar⁺ ion irradiated Au films as a function of fluences (partial spectra to emphasize the backscattering from Au are only shown)

atoms has been confirmed further by the electron microscopy measurements (Figure 6a). The microscopy results particularly support the observed backscattering results, i.e., the increase in the Rutherford backscattering yield as well as the shift in the concentration profile of Ag atoms (Figure 5) close to the glass surface. In this sample, large clusters of silver atoms (sizes ~100 to 200 nm) have been estimated. These large-scale silver nanoclusters play a dominant role in modifying the optical absorption properties. For example, intensity and the width of the surface-plasmon resonance are greatly modified, as it is clearly observed in the spectral response characteristics (Figure 6a). With increasing cluster sizes, additional higher-order (e.g., quadrupole) optical resonances become important because of the non-zero field gradient across the metal clusters. The optical results reveal a shoulder on the low wavelength side of the dipole peak. This was assigned to the quadrupolar resonance peak (inset, Figure 6a and Figure 6c).

Supported Metal Nanostructures on Glass Substrates

Ion-beam sputtering based non-equilibrium synthesis (top down approach) is a promising method leading to production of tailored nanoclusters as well as nanostructure materials on given substrates. The ion-beam sputtering based processing is also of interest because it is cost-effective compared to direct-write techniques, such as optical or electron beam lithography. Ion sputtering is a physical process whereby atoms are ejected from the surface due to bombardment of the target by energetic particles. It is driven by momentum transfer between the ions and atoms in the materials during the atomic collisions. In the present case, gold (Au) as well as silver (Ag) metallic films were deposited separately on cleaned silica substrates using the thermal evaporation set-up. Subsequently, the metal films were irradiated using the 100 keV Ar⁺ ions with various ion fluences. Rutherford backscattering experiments have been carried out to measure the areal density of Au atoms in the as-deposited Au film as well as in the ion irradiated Au film samples. Figure 7 displays the backscattering spectra of the samples. Systematic decrease

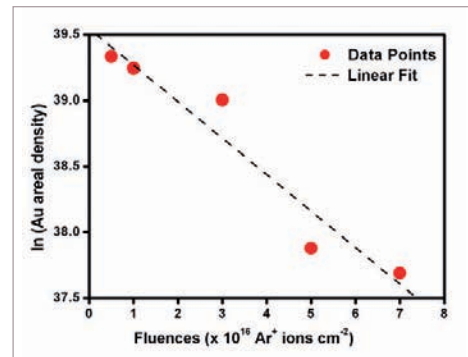


Figure 8: Log-Linear plot of areal density of Au atoms as a function of fluences of the Ar⁺ ions (experimental data points (•) are obtained from the backscattering results)

of the backscattering yield with the increase of Ar⁺ ion fluences may be observed. The decrease of area under the Au peak (which is proportional to the Au areal density) with increase of Ar⁺ ion fluences confirms the loss of Au atoms from the films due to the ion sputtering processes. This particular experimental aspect is explained here. To describe the observed experimental facts in a quantitative way in the case of sputtering of a thin film by the ion-beam, a phenomenological model equation is proposed:

$$dN_T = -kN_T d\phi \quad (2)$$

where dN_T is the reduction (due to the sputtering) of Au areal density on the substrate. Intuitively, the loss should be proportional to the instantaneous available areal density of Au atoms (N_T) and the associated increment of the ion-fluences ($d\phi$). The above differential equation is readily solved to obtain,

$$\ln(N_T) = -k\phi + c \quad (3)$$

Phenomenological constants, k and c would depend on the projectile ions, ion-beam and target material parameters. Experimentally measured areal density of Au atoms (N_T) is plotted against the respective ion-fluences (ϕ) (shown in Figure 8 as a log-linear graph). This result clearly shows that during sputtering of the Au thin films, areal density of Au atoms decreases exponentially with the increase of ion-fluences, as prescribed by the equation 3.

Presence of the metallic nanoclusters in the ion-beam sputtered samples has been elaborated through the optical absorption spectroscopy and electron microscopy results (Figure 6b and 6c). The optical response peak around 550 nm is attributed to the surface-plasmon resonance absorption in Au nanoclusters on silica substrates. Electron microscopy results show that nearly uniform size (~50 nm) of Au nanoclusters are produced on silica due to the ion-beam induced sputtering process.

Reported by P. Gangopadhyay and colleagues
Materials Physics Division
Materials Science Group

Young Officer's FORUM

Design of Elliptical Heat Exchanger for Future Fast Breeder Reactors

The commercialization of fast breeder reactor programme needs further optimization of the reactor components for the future fast reactors. A considerable portion of the total cost of the pool type fast reactor, goes into the material cost which is a function of dimensions of the main vessel, which is in turn decided by reactor internals. Main vessel dimensions are controlled by the diameter of the intermediate heat exchanger and pump in both circumferential and radial directions. Diameter of the pump is optimised for its performance; further reduction is not possible without major design changes. With the dimension of the pump as basis, the shape of intermediate heat exchanger is optimised for the most economical configuration.

A novel shape is proposed for the intermediate heat exchanger of future fast breeder reactor considering the techno-economical feasibilities. Optimization of the configuration of intermediate heat exchanger for the most economical benefit is brought out in this report along with detailed process design of intermediate heat exchanger with a design life of 60 years at 85% load factor.

The intermediate heat exchanger is a vertical counter current flow, shell and tube heat exchanger with primary sodium flowing downwards on the shell side and secondary sodium flowing upwards on the tube side. Each intermediate heat exchanger

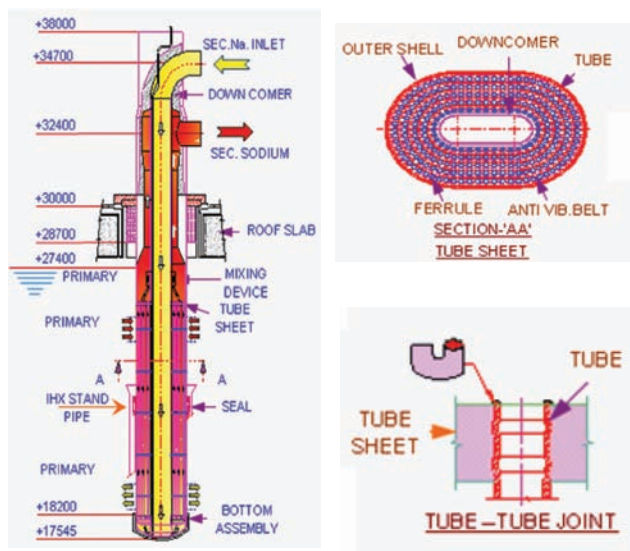


Figure 1: Intermediate heat exchanger for future fast breeder reactors



Shri V. Sudharshan took his B.E. degree in Mechanical Engineering from Andhra University. He is the Homi Bhabha Award winner for topping the Mechanical Engineering discipline from the 4th batch of BARC Training School at IGCAR and is currently Scientific Officer (C) in Reactor Components Division, Reactor Design Group. He is responsible for the design of sodium – sodium heat exchangers.

(Figure 1) is rated for 314.7 MW (t) and consists of a tube bundle having straight tubes. Each tube is 8050 mm and is made of austenitic stainless steel SS316LN, rolled and welded to the tube sheets at both the ends (Figure 1). The tubes are arranged in a circumferential pitch around an inner shell. This inner shell is welded to the tube sheets at both the ends.

Choice of Intermediate Heat Exchanger Shape

The reactor assembly proposed for future fast breeder reactors is shown in Figure 2. If the opening for the pump at the roof slab level is made to be the governing parameter for the main vessel diameter, diameter of main vessel can be further reduced by ~300 mm. This is possible based on the fact that area available for the heat transfer to take place is the parameter and not the shape of the heat exchanger especially for liquid metals. With this factor as the basis, the area available in the reactor assembly is studied for other parameters like interface of internals etc. and it is concluded that the maximum dimensions available for heat exchanger for a 500 MWe, two loop design with two intermediate heat exchanger per loop, are 2140 mm along the circumference and 1550 mm along the radial direction for the outer shell dimensions. With these dimensions, the possible configurations for intermediate heat exchanger shape are worked out and the final shapes that are considered for the study are elliptical, oval

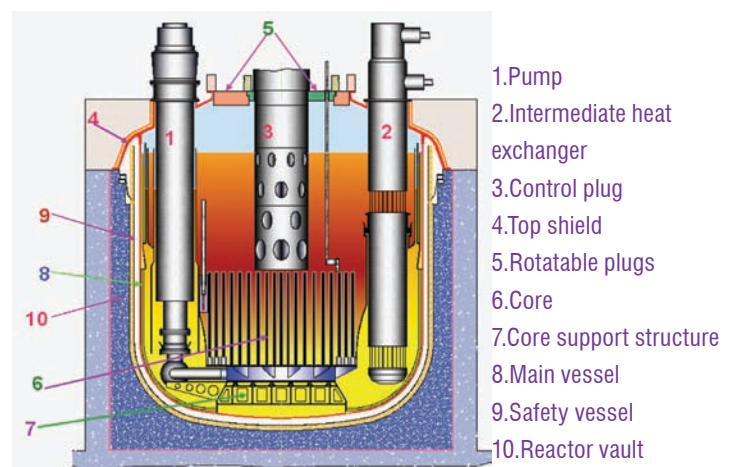


Figure 2: Reactor assembly of future fast breeder reactors

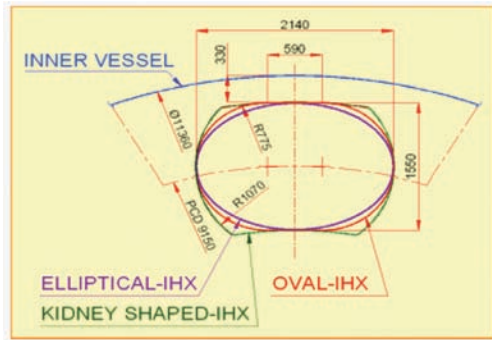


Figure 3: Comparison of possible shapes for intermediate heat exchanger

and bean/kidney as shown in Figure 3.

With two different dimensions along the axes, ellipse appears to be a natural choice, but a close examination of Figure 3 shows that by adopting kidney shape there is overall optimization of space. Kidney shape though utilises the maximum space available, is made of segments with different centres that pose problems during manufacturing. Further its advantage over the oval shape is also minimal. So the oval shape which is a simple extension of circular shape with a horizontal portion connecting two semi-circles is preferred as the shape of intermediate heat exchanger for future fast breeder reactors. With oval shape, the scheme for the ferrule and anti-vibration belt shall be retained same as that for the intermediate heat exchanger of Prototype Fast Breeder Reactor. Once the outer shell shape (shape of intermediate heat exchanger) is decided, the next parameter is to decide upon the shape of the central down comer, through which the secondary sodium enters the intermediate heat exchanger. The governing parameter for the choice of down comer is that the velocity of sodium in the down comer must be restricted to a maximum of 9.0 m/s due to erosion of structural material in intermediate heat exchanger. Since this is a limiting value, it is retained as a guiding parameter to arrive at other parameters for intermediate heat exchanger.

Design Constraints

1. Maximum pressure drop on shell side (H) = 1.45 mlc Na
2. Maximum dimension of intermediate heat exchanger outer shell (shroud) = 2140/1550 mm

The other design constraint is the maximum heat transfer length.

Table 1: Chemical composition of SS316LN (balance-iron)

Element	C	N	Cr	Ni	Mo	Si	Mn	S	P
Composition(wt%)	0.03	0.085	16	11.2	2.0	0.6	1.3	0.005	0.042

Table 2: Chemical composition of nuclear grade sodium

Impurity element	O	C	Cl	Ca+Mg	Fe
Content, ppm	<3	<25	5	70	3

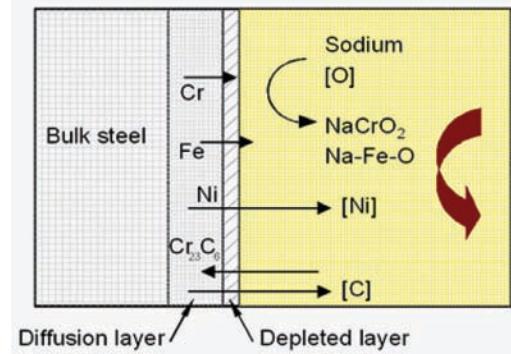


Figure 4: Overview of corrosion mechanisms in liquid sodium

This is decided to be 7.5 meter from the interface of intermediate heat exchanger with other reactor assembly components.

Thickness of Tube for 60 Year Design Life

The use of liquid metals as coolant in fast breeder reactors, introduces solid-liquid metal interactions, which are not primarily electro-chemical, as found in systems involving aqueous media. The corrosion of solid metals by these coolants occurs as the system attempts to attain chemical equilibrium. The chemical compatibility of sodium with AISI 316LN is generally good when the sodium is pure. However, the presence of impurities such as oxygen and carbon combined with a suitable velocity and thermal gradients in sodium leads to increased corrosion. The composition of SS316LN and nuclear grade sodium are shown in Tables 1 and 2. Localised electrochemical corrosion is absent in intermediate heat exchanger due to the presence of molybdenum in the steel. Liquid sodium dissolves various constituents of steel at high temperatures, which are transported and deposited in different regions at low temperature. The basic corrosion mechanisms of austenitic stainless steel in liquid sodium environment at high temperatures are:

- Complete loss of material due to leaching leading to reduction in wall thickness
- Preferential leaching of elements forming modified surface layer
- Formation of a carburised or decarburised layer below the modified surface layer depending on the carbon activity difference between sodium and steel, temperature and duration of exposure
- Precipitation of carbides in the matrix brought about by thermal effects coupled with carbon transfer in sodium

Overview of the corrosion mechanisms involved in liquid sodium corrosion is given in Figure 4.

Predominant corrosion mechanisms applicable to austenitic stainless steels in liquid sodium are the selective leaching and the steady state corrosion.

The effect of carburization on properties of SS316LN would be not very restrictive for design of intermediate heat exchanger.

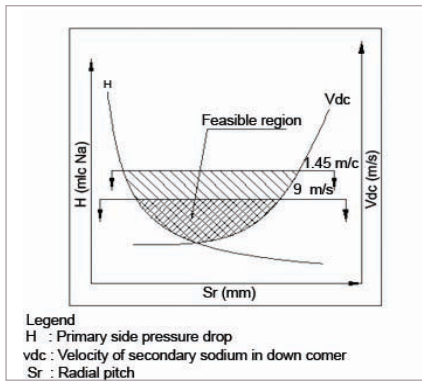


Figure 5: Graphical representation of feasibility study

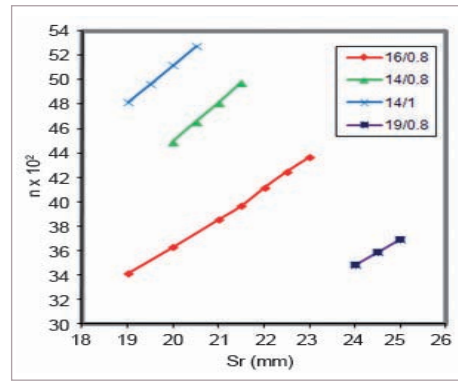


Figure 6: Variation of number of tubes in Intermediate heat exchanger as a function of radial pitch

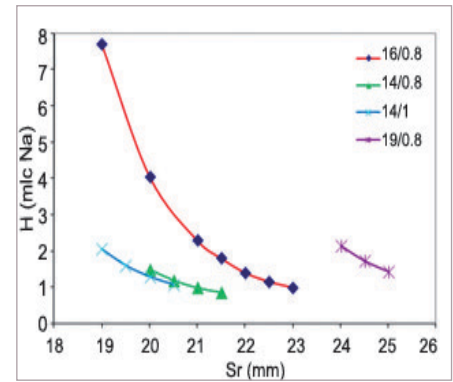


Figure 7: Variation of shell side pressure drop as a function of radial pitch

It is recommended that the corrosion allowance for 60 year design life of intermediate heat exchanger is 0.114 mm. Analysis and design of components is proceeded accordingly.

Prototype Fast Breeder Reactor intermediate heat exchanger tube thickness is 0.8 mm and margin on thickness is 0.2 mm, comprising of both corrosion allowance and negative tolerance on tube diameter (10%). Studies also show that for Prototype Fast Breeder Reactor, the unaffected base thickness of 0.6 mm is adequate for all loadings for 40 year design life. Further, optimization studies are planned to reduce the pressure transmitted to intermediate heat exchanger tube designed for 60 year design life based on 0.6 mm unaffected base thickness. Considering possible uncertainty, 0.8 and 1 mm thick tubes are selected for optimization of intermediate heat exchanger configuration.

Parametric Study on Process Design of Intermediate Heat Exchanger for Tube Selecton

A parametric study is conducted for the selection of tube size and arrangement for the specially shaped intermediate heat exchanger to check feasibility and optimization with the tube sizes (OD/THK), 14/1, 14/0.8, 16/1, 16/0.8, 19/1, 19/0.8, 24/1 mm. A computer code is written for this purpose and is validated with Prototype Fast Breeder Reactor values. Ratio of the circumferential pitch and radial pitch ($S_c/S_r = \pi/3$), which is adopted same as that for Prototype Fast Breeder Reactor, as the arrangement of tubes in the sodium to pass through is turning out to be same for any of the other configurations which are made to exploit the symmetry in the geometry of the systems which is 60° for Prototype Fast Breeder Reactor and 90° for the present intermediate heat exchanger. The study included a feasibility study for the mentioned sizes which means simultaneous satisfaction of all the design constraints and the options are further studied for optimising the convex region, which gives most economic

benefit. Results of feasibility study is shown in a graph in the Figure 5. Variation of optimization parameters with respect to tube size and radial pitch for the feasible options (tube size) are as shown in the Figures 6, 7 and 8. All the configurations are studied from OD+5 mm since at least a 5 mm ligament is required for the tube sheet to prevent tearing. Study for 16/0.8 case is carried out to with $S_r < OD + 5$ mm to study the behaviour in that range. 19/0.8 mm with radial pitch 25 mm is selected as the best suited option from economic considerations (material and manufacturing costs) for the future fast breeder reactors, the next option being 16/0.8 and 22 mm radial pitch. Table 3 gives a comparison of intermediate heat exchanger configuration for the Prototype Fast

Table 3: Comparison of intermediate heat exchanger configuration for Prototype Fast Breeder Reactor and future fast breeder reactors

Parameter	PFBR	Future FBR
Design life (Y)/cap. factor	40/75%	60/85%
Number of tubes	3600	3680
Tube diameter/thickness (mm)	19/0.8	19/0.8
Number of rows	25	23
Number of tubes in first row	72	94
Corrosion allowance (mm)	0.12	0.142
Shroud dimensions (mm)	1850	2140/1550
Area margin	24%	28%
Average primary inlet velocity (m/s)	0.377	0.362
Velocity of secondary sodium in down comer (m/s)	9.2	7.36
Shell side pressure drop (mlc Na)	1.45	1.39
Velocity of secondary sodium in down comer (m/s)	9.2	7.36
Shell side pressure drop (mlc Na)	1.45	1.39
Main vessel diameter (m)		
* with oval Intermediate heat exchanger	12.9	11.9*

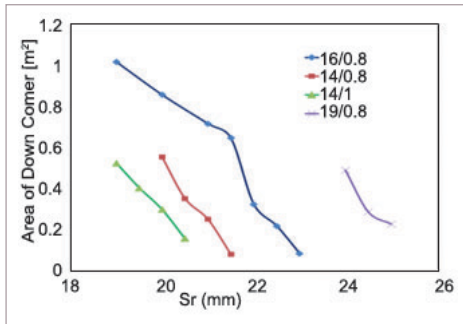


Figure 8: Variation of available down comer flow area as a function of radial pitch

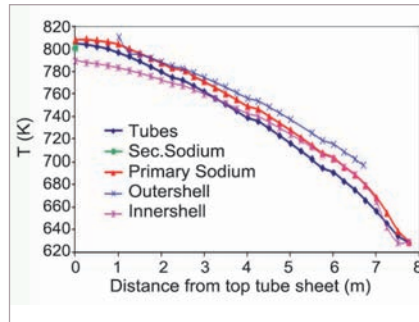


Figure 9: Average axial temperature profile in intermediate heat exchanger

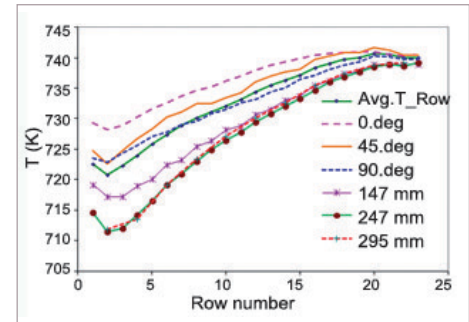


Figure 10: Radial and circumferential temperature distribution in tube bundle

Breeder Reactor and future fast breeder reactors.

Thermal Hydraulic Investigation on the Intermediate Heat Exchanger

Intermediate heat exchanger is a counter current heat exchanger with primary sodium flow on the shell side and heat transfer area is based on the outer diameter of the tube, whereas in the actual scenario heat transfer takes place by a combination of cross flow and counter current parallel flow. These 3-Dimensional features contribute to uncertainties in the design vis-a-vis assumptions, correlation, by-pass flow near shells (inner and outer shells) etc. Taking these into consideration and the possibility of plugging of a few tubes during manufacturing, it has been estimated from the CFD studies that 28% area margin on the rated value is required to overcome the uncertainties in thermal design for Prototype Fast Breeder

Table 4: Comparison of Analytical and CFD results

Parameter		Analytical Result	CFD Result	Deviation %
Heat flux	Primary	313.18 MW	319.541 MW	+ 2.03
	Secondary	313.25 MW	319.538 MW	+ 2.0
Mass flux	Primary	1649 Kg/s	1648.465 Kg/s	- 0.03
	Secondary	1450 kg/s	1450 Kg/s	0
Temperature	Primary inlet	817 K	817 K	0
	Primary outlet	667 K	664.1 K	-0.4
	Secondary inlet	628 K	628 K	0
	Secondary outlet	798 K	801.567 K	+ 0.45
Pressure drop on shell side		11479.679* Pa (1.3926 mlc) *	11456.191 Pa (1.3898 mlc)	-0.2
*Considering 10% uncertainty margin for correlations				

Reactor. The same has been adopted in the present study. Since the shape is non-circular, there is a possibility for a non-uniform flow along the circumferential direction in addition to the maldistribution of flow that is happening in the radial direction (to the shells) due to the cross flow entry of the primary sodium. There can be flow distribution along the peripheral and axial direction in the hot pool at intermediate heat exchanger inlet. In order to check the adequacy of design margin for the heat transfer owing to various uncertainties mentioned earlier, a CFD for a 90° sector model study simulating the full load operation has been carried out. Table 4 gives the comparison of analytical results with CFD results. The results confirm that the provisions in the design are sufficient for the specified rating and the pressure drop on the shell estimated using correlations and that calculated by CFD simulation are matching within a deviation of 0.2%. This sufficiently validates the analysis. Average axial temperature distribution is shown in the Figure 9. The heat transfer process in the intermediate heat exchanger at various elevations with zero meter elevation as the bottom of the top tube sheet and -7.75 meter elevation as the top of the bottom tube sheet is depicted in the graph. Outer shell is present between the two windows, starting at -1 meter elevation, spanning 5.7 meter. Figure 10 shows the average temperature of tubes estimated at six different locations along with weighted average row temperature of tube bundle.

Summary

Elliptical intermediate heat exchanger for future Fast Breeder Reactors is optimized for achieving overall economics and compactness. Detailed 3D thermal hydraulic investigations on 90° symmetry sector of intermediate heat exchanger confirms the adequacy of design margins for various process parameters such as heat transfer area, pressure drop, etc.

*Reported by V. Sudharshan
Reactor Components Division, Reactor Design Group*

Young Researcher's FORUM

Enhanced Transmission with Tunable Fano like Profile in Magnetic Soft Matter

Resonance exhibiting distinctly asymmetric line shape, well known as Fano resonance is a ubiquitous phenomenon observed in various condensed matter systems such as quantum dots, carbon nanotubes and graphene etc. The observation of the enhanced transmission with Fano shape in perforated metallic films have also attracted enormous attention due to their application in molecular sensing, spectroscopy, photonic devices etc. besides fundamental understanding. The observed enhanced transmissions, in perforated periodic and aperiodic metallic systems are attributed to surface plasmon and localized waveguide resonances, respectively. However, the exact origin of enhanced transmission and Fano resonance is still not very clear. Moreover, till now all the Fano resonances are observed only in systems with well-engineered structures. Soft matter systems like nanofluids have been a topic of intense research during the last one decade due to their interesting properties and technological applications. The issues that we tried to address here are the following: (i) can Fano resonance be realized in a smart soft matter with aperiodic or random tubes and (ii) is it possible to tune the Fano profile using external stimuli like magnetic field. We provide first experimental evidence of Fano resonance in soft matter. Under an external magnetic field, the transmittance spectrum of a ferrofluid emulsion containing oil droplet size (diameter) of ~ 220 nm (polydispersity $< 2\%$) shows an enhanced peak with Fano-like profile, which is attributed to localized waveguide resonance from random array of tubes, with charged inner surface, formed by the alignment of magnetically polarizable droplets. Further, by varying the magnetic field, the Fano profile is tuned and an opaque emulsion is turned to a transparent one. This finding will have interesting applications in tunable photonic devices.

The ferrofluid (ff) emulsion used in our studies is octane oil droplets containing magnetic (Fe_3O_4 , $d \sim 6.5$ nm) nanoparticles dispersed in water. The oil droplets are electrostatically stabilized with an anionic surfactant of sodium dodecyl sulphate. On applying an external magnetic field H_0 , the strength of interaction between the droplets increases, which is described by the



Mr. Junaid Masud Laskar did his Masters in Physics from Tezpur University, Assam. He is the University third rank holder for M.Sc. He joined as a research fellow in January 2006 under the guidance of Dr. John Philip, Head, SMARTS, MMG and has submitted his Ph.D thesis in September, 2011 to the University of Madras. The title of his thesis is "Probing of Structural Transitions in Magnetically Polarizable Soft Matters by Light Scattering". He has published eight papers in reputed international journals. He has attended six international conferences and won the best poster presentation award at Second International Conference on Frontiers in Nanoscience and Technology, Cochin. Presently, he is pursuing his post doctoral research at the prestigious Max Planck Institute for Polymer Research, Mainz, Germany.

coupling constant $\Lambda = \pi\mu_0 d^3 \chi^2 H_0^2 / 72k_B T$ where χ and $k_B T$ are the magnetic susceptibility and thermal energy respectively. When $\Lambda > 1$, the emulsion undergoes disorder-order structural transition, where linear chain-like structures are formed due to head on aggregation of oil droplets along H_0 . To obtain insight into the implications of field induced structures, the transmitted light intensity is recorded as a function of H_0 at different ramp rates using an automated light scattering set-up. The ff emulsion of volume fraction $f = 0.0033$ is observed to be opaque to red light (He-Ne Laser, $\lambda = 632.8$ nm) for cuvette of path length $L = 1$ mm. This scattered light emerges from the exit face of the cuvette in the form of a cone, which originates from the scattering of incident light from the cylindrical surface of field induced chains. Figure 1(a) shows the images of the exit face of the cuvette that contains the sample, at different H_0 . The intersection, of this cone of scattered light, on a screen placed at far field and perpendicular to the incident light forms a ring like pattern as shown in Figure 1 (c). A bright spot is also observed on the upper right

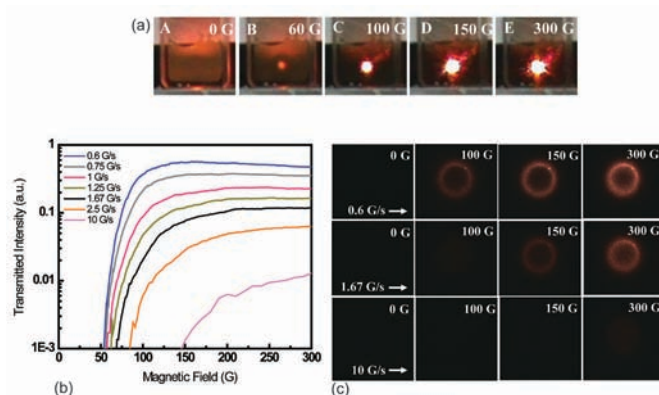


Figure 1: (a) Images of transmitted light as a function of magnetic field during increase (ramp rate ~ 0.6 G/s) just at the exit face of quartz cuvette, which contains the ferrofluid emulsion, (b) Variation of transmitted light spot [top right corner of ring circumference of (c)] intensity during increase in magnetic field for different ramp rates, (c) Scattered patterns at four different fields during the increase at three ramp rates of 0.6, 1.67 and 10 G/s

part of ring circumference, which is the transmitted light spot in the direction of incident light. Figure 1(b) shows the intensity variation of this transmitted light spot as a function of increasing H_0 at different ramp rates. The emulsion remains opaque to the incident light upto a H_0 of 50 G, above which the transmitted intensity increases with the increase in H_0 . For low ramp rate (0.6 G/s), the transmitted intensity again decreases above 150 G with increase in H_0 .

Considering the emulsion as a system of random scatterers, the transmitted light intensity for a path length L is given by $I_t = I_0 \exp(-nQ_{ext}\pi a^2 L)$ where I_0 , a , n and Q_{ext} are the incident light intensity, scatterer radius, scatterer number density, scattering extinction efficiency respectively. The Q_{ext} is calculated using Mie scattering theory as a function of size parameter (ka) and is found to be very high for the ferrofluid emulsion, where the scatterer (oil droplet) radius $a=110$ nm i.e. $ka=1.45$. At $H_0=0$ G, the calculated incident light transmitted intensity I_t/I_0 for the given system is found to be very small ($\sim 2.9113 \times 10^{-46}$). Therefore, significant scattering from the oil droplets in the emulsion forbids the light transmission in the absence of any magnetic field.

On application of H_0 , due to the aggregation of oil droplets, the internal structure inside the ferrofluid emulsion looks like array of random tubes (diameter $D \sim \lambda$) as shown in Figure 2. Now, the behavior of light transmission as a function of H_0 , through the above mentioned structural arrangement, is basically influenced by two factors. First, the effect of change in light scattering due to changing chain length and secondly, the effect of changing dimensions of tubes, both tube diameter (D) and tube length (z). With the increase in H_0 , due to the increase in chain length by the aggregation of oil droplets, the space between the chains i.e. the tube diameter also opens up.

This structural rearrangement takes place for the uniform distribution of the field induced structures through out the entire volume of the sample. In fact due to opening up of the tubes and increase in their diameter, effective scattering cross section of

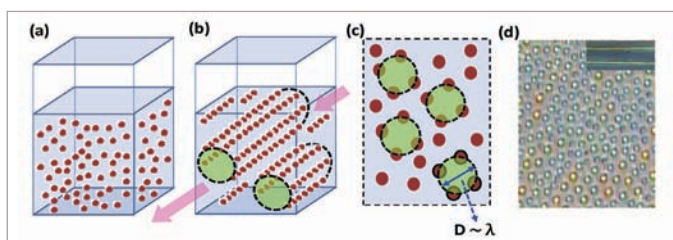


Figure 2: Schematic of ff emulsion at (a) $H_0 = 0$ G, (b) $60 \text{ G} < H_0 < 300 \text{ G}$, the array of chains and tubes and their dimensional variation as function of external magnetic field strength, arrow shows the direction of incident light and magnetic field, (c) cross sectional view of field induced tubes; (d) optical microscopic image of the cross sectional view of chains under external field, inset shows the chain formation along the field direction

the system decreases, which results in increase in transmitted light, thereby making the transition of the system from opaque to transparent above 50 G as shown in Figure 1(b). Therefore, it is clear from this observation that the above mentioned second factor dominates over the first one on the light transmission behavior under external field.

The specialty of the field induced tubes are discussed in detail further. Because of the negatively charged anionic head group of surfactant sodium dodecyl sulphate and free π electrons present, the inner tube surfaces are highly charged with a typical charge density $500 \mu\text{C}/\text{cm}^2$ ($10^{12}/\text{cm}^2$ in terms of electron number density), so that electric and magnetic fields of incident electromagnetic wave cannot penetrate the inner surface, thereby making the tubes behave like waveguides. Now, the system looks like an array of aperiodic random tube waveguides, whose dimensions are function of H_0 . The transmitted wave amplitude decreases exponentially along the waveguide as $\exp(-\alpha_w z)$ due to the finite impedance of inner charged walls of the waveguide, where α_w and z are the waveguide damping coefficient and waveguide length respectively. This causes the decrease of transmitted intensity with the increase in z , on increasing H_0 [above 150 G for 0.6 G/s in Figure 1 (b)]. Therefore, opening of tubes and increase in their 'D' cause the initial transition of the system from opaque to transparent around 50 G as shown in Figure 1(b). Whereas, the decrease of transmitted intensity above 150 G for 0.6 G/s is caused by the increase in 'z'.

The aggregation time (t_c), at a given H_0 depends on the competition between the magnetic force and viscous force experienced by the oil droplets in the carrier liquid. This t_c is the time required for aggregation of two oil droplets of radius 'a' containing the magnetic nanoparticles, when they are separated by a distance 'r' in a medium with viscosity ' η '. For lower ramp rates, external field exposure time is longer and sufficient ($> t_c$) so that the tubes can attain the maximum permissible dimensions (by aggregation of oil droplets) for a given H_0 . Therefore, both the diameter of the tubes and the proportion of the number of tubes to single chains increases as the external field ramp rate is decreased. This is also the reason why the tube waveguide transmission behavior plays a prominent role on transmitted intensity variation at low ramp rate (0.6 G/s). For higher ramp rates (field exposure time $< t_c$), only short chains are able to form, which are unable to arrange themselves to form tubes. The scattering effect by the short field induced chains dominates on the transmitted intensity output and therefore, it does not reach its equilibrium saturation value.

The experiments mentioned above are also carried out while decreasing the H_0 , immediately after reaching the maximum field (300 G), at the same ramp rate at which it is increased. Figure 3(b) shows the scattered pattern images, on a screen placed perpendicular to the incident light, but during

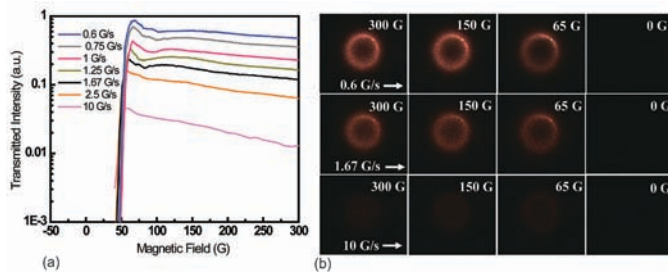


Figure 3: (a) Variation of transmitted light spot intensity during decrease in magnetic field at different ramp rates and (b) scattered patterns at four different fields during the decrease at three ramp rates

the decrease in H_0 at ramp rates of 0.6, 1.67 and 10 G/s. Figure 3(a) shows the intensity variation of the transmitted light spot [upper right part of ring circumference of Figure 3(b)] as a function of decreasing H_0 . During the decrease in H_0 , the transmitted intensity increases unusually and peaks at 68 G before falling sharply to zero value below 50 G. When H_0 is decreased at 0.6 G/s, the ring structure gradually disappears and intensity of the transmitted spot on its circumference reaches its maximum at 68 G before complete disappearance [Figures 3(a & b)]. We attribute the enhanced transmission peak observed for the field induced array of random tubes to the localized waveguide resonances related to individual tubes.

To get further insight into the observed enhanced transmission, the zero order transmittance spectra of the emulsion at different H_0 during the decrease in field (ramp rate \sim 0.6 G/s) are recorded using a fiber optical spectrophotometer and is shown in Figure 4. With the decrease in H_0 , the transmittance of the emulsion increases for the entire range of wavelengths ($\lambda=450-800$ nm). Besides, an enhanced asymmetric peak is also observed in each transmission spectrum, which shows a red shift with the decrease in H_0 . The transmittance spectra for $H_0 = 0$ i.e. the disordered system of scatterers can be explained from the calculation of Q_{ext} using the Mie scattering theory. For $\lambda = 450-800$ nm, $ka=2.04-1.15$, the corresponding Q_{ext} is significantly high (3.65-1.48) which results in very less transmittance I_t/I_0 ($\sim 2.155 \times 10^{-36} - 3.451 \times 10^{-15}$). But, for λ in the range 800-1000 nm ($ka=1.15-0.91$), Q_{ext} decreases from 1.48 to 0.58, thereby reducing the scattering or increasing the fraction of incident light intensity that is transmitted, I_t/I_0 ($\sim 3.451 \times 10^{-15} - 2.15 \times 10^{-6}$).

The transmittance over the entire wavelength range increases with the decrease in H_0 , due to the deaggregation of oil droplets, the length 'z' of the tubes decreases on decreasing the field. This increases the number of tubes and therefore decreases their D. This arrangement takes place for the uniform distribution of the field induced structures throughout the entire volume of the ferrofluid emulsion, so as to reach the minimum energy state. The fractional aperture area can be considered to remain more or less the same after the redistribution of the tubes at different

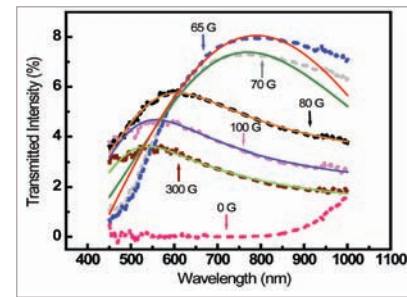


Figure 4: Transmittance spectra of the ff emulsion at different magnetic fields when decreased at a ramp rate of 0.6 G/s from 300 G. The solid lines are the best fits obtained using Fano resonance profile

H_0 . For a given fractional aperture area of an array of aperiodic waveguides, the transmittance increases with increase in the number of tubes.

The reasons for the red shift of asymmetric peak, observed in the transmittance spectra, on decreasing H_0 , enumerated below. The light transmission process, through an array of tube waveguides with their dimensions in the subwavelength regime or of the order of the wavelength of incident electromagnetic wave, involves two interfering contributions propagating through two different scattering paths. The first path is non-resonant and is related to direct scattering of the incident light field through the waveguides. The observed non-resonant transmittance variation can also be characterized well by the extension of Bethe-Bouwkamp theory, for a circular hole waveguide with negligible thickness in a perfectly electrical conducting film, to that with definite thickness and real metal. The non-resonant transmission continuum of direct scattered states related to individual waveguides is detected as background in the transmission spectra. The second path corresponds to a resonant contribution, as it first goes through the localized resonance state of the waveguide before being scattered to outside continuum. The interference between the transition amplitudes associated with each scattering path gives the resulting light transmittance with an asymmetric peak in the spectra, known as Fano resonance as shown in Figure 4. The transmittance spectra have been fitted with the functional form of Fano resonance $I \propto \frac{(F\gamma + \omega - \omega_0)^2}{[(\omega - \omega_0)^2 + \gamma^2]}$ and variation of the fit parameters ω_0 , F and γ as a function decreasing H_0 are shown in Figure 5. The actual resonance position i.e. the resonant wavelength (ω_0) of Fano resonance in the transmission spectra appears near the waveguide cut-off wavelength (λ_c) for single hole, array of aperiodic and periodic holes in a conducting film.

For a circular hole waveguide in a perfectly electrical conductor film, $\lambda_c = 3.4r$, where r is the hole radius. The ω_0 that appears around this λ_c shows a red shift with the decrease in waveguide length, which is demonstrated both numerically in perfectly conducting film, real metal and experimentally in single hole in a metal (Ag) film. Therefore, we attribute the red shift of ω_0 [Figures 4 & 5], to the decrease in tube length z on decreasing

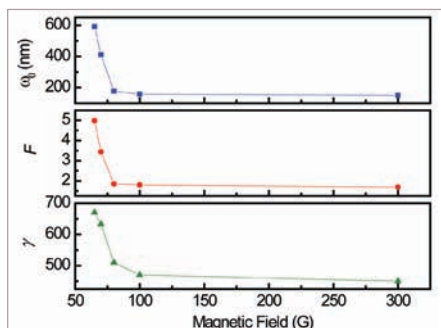


Figure 5: Fano resonance fit parameters ω_0 , F and γ as a function of external magnetic field H_0 (during decrease)

H_0 . Interestingly, for H_0 of 70 G, the extracted value of ω_0 is the incident light wavelength (633 nm) at which the resonantly enhanced transmission is also observed almost at the same field (68 G) [Figure 3 (a)], which corroborates our argument of transmission resonance to the localized waveguide resonance. The λ_c of a waveguide is directly related to its lateral dimension ('D' in the case of tube). Though the ω_0 of a waveguide is of the order of its λ_c , the exact resonance position depends on the 'z' of the waveguide. The resonant wavelength, for the circular hole waveguide, coincides exactly with the cut off wavelength for the waveguide length $z=r/3$. Therefore, the observed red shift of resonance position (ω_0) in the transmittance spectra [Figures 4 & 5] also shows that on decreasing H_0 , the effect of decreasing 'z' dominates over the decreasing 'D', on determining the resonance peak position. Further, on decreasing H_0 , at first 'z' decreases by deaggregation of oil droplets from the chains. Then, the spatial rearrangement takes place for the uniform distribution of the field induced structures throughout the entire volume resulting in the decrease of 'D', so as to reach the minimum energy state. Therefore, the rate of decrease in 'z' is faster than their 'D', thereby making the effect of decreasing 'z' more prominent on ω_0 .

The discrete localized state corresponding to the resonant state of a waveguide depends on its dimension. At higher H_0 (e.g. 300 G), due to high coupling constant Λ , there is very less dimensional distribution ($z \pm \Delta z$ & $D \pm \Delta D$) of the waveguides. On decreasing H_0 , this dimensional distribution increases along with the decrease in 'z' and 'D', as mentioned earlier. This leads to increase in the number of discrete resonant states of the random array of field induced tube waveguides. Therefore, the transition amplitude associated with the resonant scattering path i.e. the discrete localized states, increases as compared to non-resonant direct scattering path as mentioned earlier. The increase in the ratio of these two transition amplitudes, defined as the asymmetry parameter F, with the decrease in H_0 , as shown in Figure 5, demonstrates this phenomenon. The actual resonant wavelength (ω_0) lies somewhere between the observed maximum and minimum of the asymmetric transmittance spectra indicated in Figure 4 and the value of parameter F defines the relative deviation. In the situation $|F| \rightarrow \infty$, the ' ω_0 ' coincides with the maximum

of the spectra, for $F=0$ the ω_0 coincides with minimum and for $F=1$ it is located exactly half the distance between the maximum and minimum of the spectrum. With the increase in the value of F, as H_0 is decreased, the ω_0 for a transmittance spectrum shifts more towards its maximum. This is also evident from the extracted values of ω_0 [Figure 5] in the observed transmittance spectra [Figure 4] for different H_0 .

The non-resonant background in the transmittance spectra depends on the number of tube waveguides, their dimensions (z & D) and their dimensional distribution ($z \pm \Delta z$ & $D \pm \Delta D$) at a particular H_0 . On decreasing H_0 , if only the 'z' would have changed while keeping the other factors constant; only a red shift of transmittance resonance position (ω_0) with similar background would have been observed, as discussed earlier. At the resonance, the phase of the scattering wave changes sharply by π . Thus, the interaction of scattering waves results in constructive and destructive interference phenomena located very close to each other, corresponding to a maximum E_{\max} and minimum E_{\min} of the transmission, respectively. The width of the resonance is proportional to the distance between them, $\gamma \sim |E_{\max} - E_{\min}|$. Due to the increase in the number discrete localized states of the array of random waveguides with the decrease in H_0 , the number of possible resonant scattering paths to the continuum through these states also increases. This leads to an increase in the number of possible interferences among the transition amplitudes corresponding to different resonant scattering paths. Since each of these interferences has both constructive and destructive interferences, it results in the occurrence of many resonances. This leads to the observation of many overlapped resonances in a single transmittance spectrum and increases the width of transmittance spectra when H_0 is decreased, as demonstrated by the increase in γ [Figures 4 & 5]. Note that similar broad Fano transmission resonance with changing background is also observed for an array of aperiodic uncorrelated holes on a conducting film. Therefore, the increase in transmittance and red shift of the resonance position (ω_0), observed on decreasing H_0 , indicates that the decrease in 'z' has the dominant contribution over other field dependent variable parameters on the resulting transmitted intensity behavior through the field induced array of randomly uncorrelated tube waveguides in the emulsion. Whereas, the increase in asymmetry parameter F and resonance width (γ), observed on decreasing H_0 , indicates that the increase in dimensional distribution ($z \pm \Delta z$ & $D \pm \Delta D$) of the tube waveguides also plays significant role on the resulting transmitted intensity behavior. On decreasing the H_0 below 65 G, Λ becomes less than unity, which leads to complete dissolution of the field induced structures.

*Reported by Junaid Masud Laskar
Smart Materials Section
Metallurgy and Materials Group*

Conference/Meeting Highlights

Theme Meeting on Severe Accident Analysis and Experiments

April 26-27, 2012



Panel members Shri H. G. Lele, RSD, BARC, Shri S.S. Bajaj, Chairman, AERB, Shri S. K. Mehta, Former Director, Reactor Group, BARC, Prof. K. Iyer, Mechanical Engineering Department, IIT Bombay, Dr. P. Chellapandi, Director, RDG, IGCAR and Shri P. K. Malhotra, NPCIL on the dais

Following the Fukushima events, there is a need to review and re-assess the strategies adopted in various nuclear facilities for severe accident management. This is essential for evolving a robust accident mitigation and management guideline for all future nuclear reactors. A theme meeting was organized by SRI-AERB in collaboration with IGCAR, at Anupuram during April 26-27, 2012 with an aim to take a consolidated look at the current status of on-going analytical and experimental research work on various aspects of severe accident management, within the DAE units as well as at academic institutions. It is envisaged that the outcome of the deliberations would provide the necessary thrust and direction in focusing research activities in challenging areas and reorient collaborative

research activities among the participating organizations. Shri S.S. Bajaj, Chairman, AERB, in his introductory remarks, indicated that events at Fukushima have changed the perspective of nuclear communities' in responding to such events and evolving mitigating measures. Shri S.K. Chande, Vice Chairman, AERB delivered the key note address highlighting the shift in focus and practices in safety subsequent Fukushima. A total of twenty lectures were delivered by eminent invited speakers from various R&D organizations and academic institutions, on a wide range of issues relating to R&D on severe accidents in thermal as well as fast reactors. The theme meeting was concluded with a panel discussion chaired by Shri S. K. Mehta, Former Director, Reactor Group, BARC.



Shri S.K. Chande, Vice Chairman, AERB delivering the key note address

Reported by Seik Mansoor Ali, SRI, AERB

Theme Meeting on Robust Instrumentation and Control for Nuclear Facilities (RINF-2012) May 29, 2012



Dr. P. R. Vasudeva Rao, Director, Chemistry Group, IGCAR inaugurating the theme meeting. Shri S. A. V. Satya Murty, Director, EI&RSG, IGCAR, Shri C. K. Pithawa, Head, Electronics Division, BARC and Shri D. Thirugnanamurthy, EID, IGCAR are on the dais

A one day theme meeting on "Robust Instrumentation and Control for Nuclear Facilities" (RINF-2012) was organised by Indira Gandhi Centre for Atomic Research at Sarabhai Auditorium, Homi Bhabha Building, Kalpakkam on May 29, 2012. The theme meeting started with welcome address by Shri S. A. V. Satya Murty, Convenor, RINF-2012 and Director, Electronics, Instrumentation and Radiological Safety Group, IGCAR.

Shri S. A. V. Satya Murty highlighted the importance of the theme meeting particularly in the context of development of robust instrumentation for nuclear facilities and welcomed the eminent speakers, delegates from IGCAR, BARCF, BHAVINI and MAPS.

Dr. P. R. Vasudeva Rao, Director, Chemistry Group inaugurated the theme meeting. He highlighted the vital role of instrumentation and control with respect to safety and availability of the nuclear reactor. He emphasized how important it is to provide robust and reliable instrumentation for nuclear facilities. He stressed the need for paying attention to design and the importance of redundancy. He mentioned

the challenges faced because of fast developments in the field of electronics and computers and resultant obsolescence. Shri C. K. Pithawa, Head, Electronics Division, BARC delivered the keynote address on 'Neutron detectors for Prototype Fast Breeder Reactor'. He explained the methodology followed in designing the neutron detectors to work at very high temperatures for fast reactors, the challenges faced and their solutions to overcome.

In the theme meeting, there were six invited talks by eminent professionals from IITM, Centre for Reliability, CEMILAC, BARC, ECIL and Ansh Technologies highlighting the various qualification methods to be followed in building robust instrumentation and control for nuclear facilities. The meeting was attended by more than one hundred and fifty delegates from IGCAR, MAPS, BHAVINI and BARC Facilities. There were excellent scientific interactions during the technical sessions. Shri D. Thirugnanamurthy, EID, Secretary, RINF-2012 proposed the vote of thanks.

Reported by S. A. V. Satya Murty, Convenor, RINF-2012

Theme Meeting on Technological Advancement in Production of Enriched Boron for the Control Rods of Fast Reactors

June 22, 2012



Shri S.C Chetal, Distinguished Scientist and Director, Indira Gandhi Centre for Atomic Research, presenting the inaugural address

A one day theme meeting on “Technological Advancement in Production of Enriched Boron for the Control Rods of Fast Reactors” was organized by Indira Gandhi Centre for Atomic Research, Kalpakkam and Board of Research in Nuclear Sciences, (BRNS) Mumbai at the Sarabhai Auditorium, Homi Bhabha Building, IGCAR on June 22, 2012. The meeting started with the welcome address by Shri K.K.Rajan, Chairman, organizing committee and Director, Fast Reactor Technology Group. Shri K.K.Rajan highlighted the relevance of the theme meeting in the context of the Indian fast breeder reactor programme and welcomed the invited speakers, delegates and guests. He lauded the efforts of Shri R.Subramaniam, Former Head of Chemical Technology Section at IGCAR who laid the foundation for the boron enrichment program at IGCAR and Dr. C. Anand Babu, Associate Director, Component Development Group for his contributions in leading the research and development programme for boron enrichment. Shri S.C Chetal, Director, IGCAR inaugurated the theme meeting and in his inaugural address outlined the importance of enriched boron carbide as absorber rod material for control of fast reactors. He also informed that boron carbide pellets to be used in the control rods of PFBR are ready for shipment at BARC. He reiterated that the development of this technology is a culmination of the combined efforts of BARC, IGCAR and HWB. He stressed the need to initiate research and development for recycling the enriched boron carbide from the used control rods of fast reactors. During the meeting 5 kg of 90 percent

enriched boric acid powder produced at the boron enrichment plants at IGCAR was handed over to Shri K.Nagarajan, Associate Director, Chemistry Group for further processing in the inaugural session.

Dr. C. Anand Babu in his key note address detailed the road map of the boron enrichment in the country. He particularly recalled the uphill challenges and hurdles that were overcome in achieving the present level of technological maturity. In the theme meeting there were eight invited lectures. The lectures were organized into three different technical sessions as process development for boron enrichment, technology development for conversion to enriched elemental boron and production and operating experience on absorber materials. The lectures were delivered by experts in this field from IGCAR, BARC and Heavy Water Board. Engineers from the various groups of IGCAR, BHAVINI, BARC facilities, academic institutions and industries like THERMAX were also participants to this theme meeting. There were a total of 90 participants for the theme meeting. The scientific interactions during the technical sessions were beneficial and provided valuable inputs for the design, performance assessment and further improvement of the processes in the production of enriched boron for fast reactors. The meeting concluded with a vote of thanks by Dr. B.K.Sharma, Chairman, Technical committee.

Reported by G. Padmakumar, Convenor

Visit of Dignitaries



Honorable Justice Shri S. Tamilvanan from Madras High Court and Prof. V. Manimozhi during their visit to the Fast Breeder Test Reactor

Honorable Justice Shri S. Tamilvanan from Madras High Court accompanied with his wife Prof. V. Manimozhi visited the Centre on April 14, 2012. During the meeting they were briefed about the challenges and opportunities of Atomic Energy by Dr. M. Sai Baba, Associate Director, Resources Management Group. After the meeting Honorable Justice Shri S. Tamilvanan and Prof. V. Manimozhi visited the Fast Breeder Test Reactor and Madras Atomic Power Station.

Awards & Honours

Dr. K. Gireesan and Dr. T. S. Radhakrishnan from MSG and collaborators at CIPET-Chennai, have received the 2nd National Award (2011) for Technology Innovation under the category, Polymers in Public Health Care, instituted in various fields of Petrochemicals and Downstream Plastic Processing Industry by the Department of Chemicals and Petrochemicals, Government of India, for their work on the "Design and Development of Sensor array Hemet for whole Head Magnetoencephalography System"

Dr. M. Vijayalakshmi from MMG has been elected, Fellow of the Electron Microscopy Society of India in recognition of her outstanding scientific contributions in the field of "Electron Microscopy".

Best Paper / Poster Awards

Embedded-System Based Controller for Measuring Displacement of Reactor Vessel of FBTR

Shri Kalyan Rao Kuchipudi, Shri Sushant Patil, Shri S. Sridhar, Shri M. Muthukrishnan, Shri K. V. Sureshkumar, Shri S. Varadharajan, Shri B. Anandapadmanaban and Shri G. Srinivasan from ROMG

8th Control and Instrumentation System Conference (CISCON 2011) Manipal University, Manipal, November 2011

Best Paper Award

Effective Nondestructive Imaging of Defects in Engineering Components

Dr. B. P. C. Rao, Dr. T. Jayakumar, Shri S. Thirunavukkarasu, Shri W. Sharatchandra Singh, Shri G.K. Sharma, Shri Anish Kumar and Dr. C. Babu Rao from MMG

18th World Conference on Nondestructive Testing, Durban, South Africa, April 16-20, 2012

Best Presentation Award

Logic Modeling and Benchmark Transients Simulation of Condensate System for Prototype Fast Breeder Reactor Operator Training Simulator

Ms. Rashmi Nawlakha, Ms. N. Jasmine, Ms. H. Seetha, Shri B. Subba Raju, Shri K.R.S. Narayanan, Ms. T. L. Priyanka, Ms. T. Jayanthi and Shri S.A.V. Satya Murty from EI&RSG

International Conference on Recent Advances in Engineering and Technology (ICRAET-2012)

Hyderabad, April 29-30, 2012

Best Paper Award



Cassia fistula (Golden shower tree)



Dr. M. Sai Baba,

Chairman, Editorial Committee, IGC Newsletter

Editorial Committee Members: Dr. K. Ananthasivan, Shri M.S. Chandrasekar, Dr. N.V. Chandra Shekar, Dr. C. Mallika, Shri K. S. Narayanan, Shri V. Rajendran, Dr. Saroja Saibaba and Dr. Vidya Sundararajan